Paleoceanography and Paleoclimatology

RESEARCH ARTICLE
10.1029/2017PA003235

Key Points:
- Clay minerals in the South China Sea present clear millennial-scale changes of the East Asian summer monsoon during the last glaciation
- The East Asian monsoon responds to abrupt climatic changes occurred in high latitudes via contemporaneous chemical and physical weathering
- Millennial-scale climatic changes recorded in the South China Sea terrigenous sediments are better preserved in deeper-water environments

Supporting Information:
- Supporting Information S1
- Data Set S1

Correspondence to:
Z. Liu,
lzhifei@tongji.edu.cn

Citation:
Zhao, S., Liu, Z., Colin, C., Zhao, Y., Wang, X., & Jian, Z. (2018). Responses of the East Asian summer monsoon in the low-latitude South China Sea to high-latitude millennial-scale climatic changes during the last glaciation: Evidence from a high-resolution clay mineralogical record. *Paleoceanography and Paleoclimatology*, *33*, 745–765. https://doi.org/10.1029/2017PA003235

Received 31 AUG 2017
Accepted 14 JUN 2018
Accepted article online 21 JUN 2018
Published online 14 JUL 2018

Responses of the East Asian Summer Monsoon in the Low-Latitude South China Sea to High-Latitude Millennial-Scale Climatic Changes During the Last Glaciation: Evidence From a High-Resolution Clay Mineralogical Record

Shaohua Zhao[1], Zhifei Liu[1], Christophe Colin[2], Yulong Zhao[1], Xingxing Wang[1], and Zhimin Jian[1]

[1]State Key Laboratory of Marine Geology, Tongji University, Shanghai, China, [2]Laboratoire Géoscience Paris Sud, UMR 8148 CNRS-Université de Paris-Sud, Orsay, France

Abstract High-resolution clay mineral assemblage combined with Nd and Sr isotopic compositions of Core MD12-3434 located in the northern South China Sea was investigated to reveal terrigenous sediment response to the East Asian monsoon evolution during the last glaciation. Clay mineralogical variations indicate clear millennial-scale oscillations that are mainly due to rapid changes in the proportion of smectite to illite and chlorite. Smectite is derived predominantly from rapid chemical weathering of volcanic rocks in Luzon under strong summer monsoon, while illite and chlorite are mainly sourced from Taiwan through reinforced physical erosion. Thus, the smectite/(illite + chlorite) ratio is adopted to reconstruct the East Asian summer monsoon evolution during the last glaciation. Rapid increases in the smectite/(illite + chlorite) ratio imply strengthened summer monsoon occurred during Dansgaard-Oeschger and Bølling-Allerød interstadials. In contrast, rapid decreases in the ratio indicate relatively weakened summer monsoon happened during Heinrich and Younger Dryas stadials. These millennial-scale climatic signals documented by clay mineralogical compositions of deep-sea sediments in the South China Sea can be better preserved in calm deeper-water sedimentary environments. Our study highlights the prompt responses of the East Asian monsoon system to millennial-scale climatic changes occurred in high-latitude Northern Hemisphere through contemporaneous chemical weathering of volcanic rocks and/or sediment supply variations under strong physical erosion in the low-latitude South China Sea, implying an atmospheric teleconnection from the North Atlantic to the Asian monsoon region.

Plain Language Summary This study presents the first deep-sea high-resolution clay mineralogical result to show the low-latitude East Asian monsoon system that actually responds to millennial-scale changes in high-latitude Northern Hemisphere. The mechanism is clay minerals as chemical weathering products on the Earth's surface to be contemporaneously affected from the global and regional climate changes. This study also indicates that millennial-scale climatic signals documented by clay minerals can be better preserved in deep and calm sedimentary environments to avoid interruptions of potential deep-sea sedimentary dynamic processes like contour currents.

1. Introduction

Global climate during the last glaciation is characterized by hemispherically asynchronous millennial-scale oscillations (e.g., Blunier et al., 1998; Markle et al., 2017). The repeated warm interstadials and cold stadials named Dansgaard-Oeschger (DO) and Heinrich (H) events, including Younger Dryas (YD) and Bølling-Allerød (BA), were pronounced and mostly occurred on Greenland and across the Northern Hemisphere (Bond et al., 1993; Dansgaard et al., 1993; Heinrich, 1988). Through prompt reorganizations of both oceanic and atmospheric circulations (e.g., Markle et al., 2017; Schmidt et al., 2012), such millennial-scale climate changes have a strong influence on the prevailing monsoon system on the tropical and subtropical regions (Cheng et al., 2016; Deplazes et al., 2013; Peterson et al., 2000; Sun et al., 2012; Tjallingii et al., 2008; Y. J. Wang et al., 2001, 2008). Unlike the other monsoonal systems, the East Asian monsoon contains two recognizable components, that is, a normal low-latitude summer monsoon and a unique midlatitude winter monsoon (Figure 1a). During the last glaciation, numerous studies have indicated that both components of the East Asian monsoon are characterized by clear millennial-scale variations, which are well established in loess (e.g., Guo et al., 1996; Porter & An, 1995; Sun et al., 2012) and stalagmites on lands

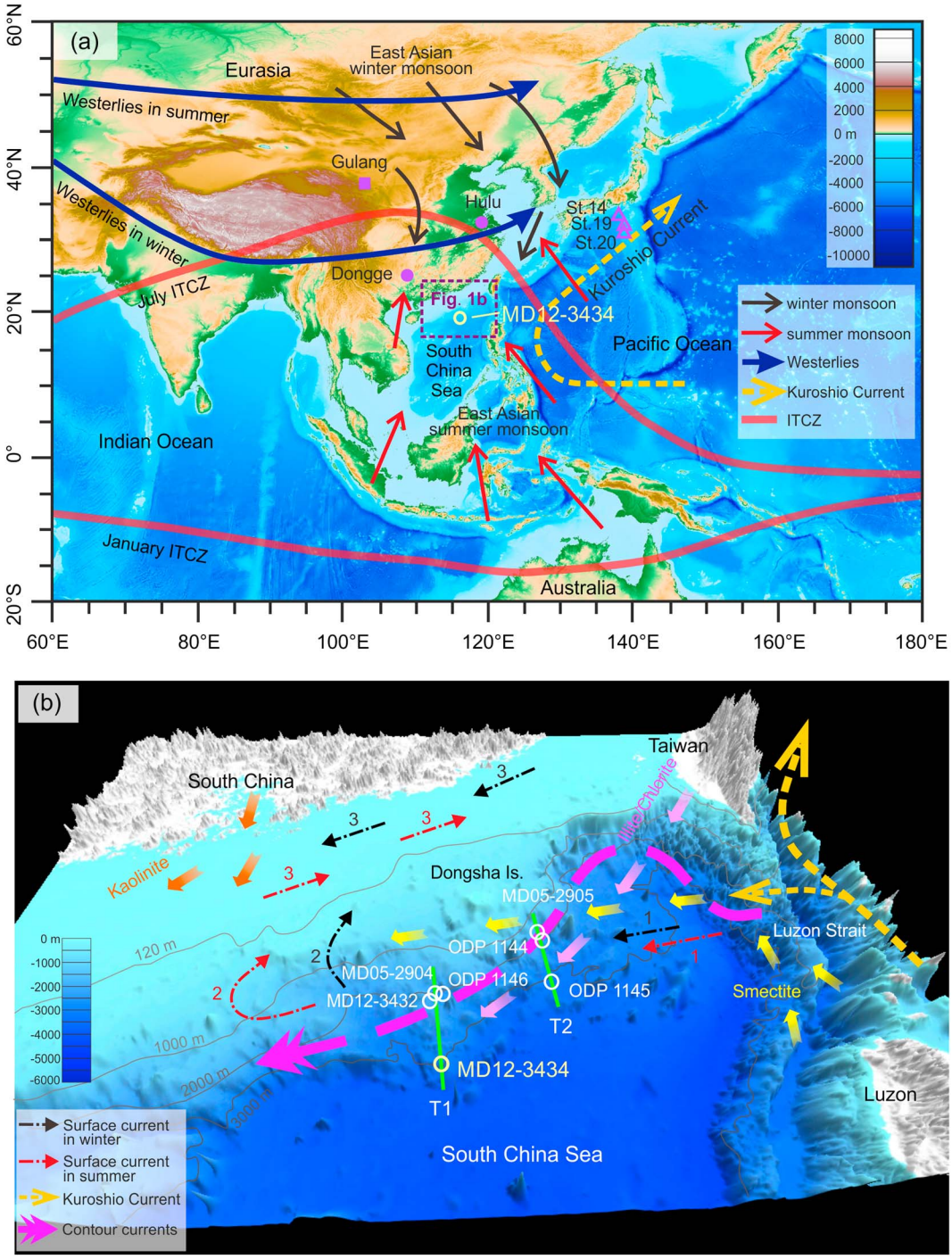

Figure 1. (a) Modern atmospheric circulation in East Asia and location of Core MD12-3434 in the northern South China Sea (SCS) as well as the locations of referenced Gulang loess profiles, Hulu and Dongge caves, and Japan coastal sediment cores St.14, 19, and 20. Modern locations of the Intertropical Convergence Zone (ITCZ) in July and January are indicated by the bold light-red lines, while modern locations of westerlies in summer and winter seasons are also presented by deep-blue arrows. (b) Oceanic current systems and clay mineral transport processes in the northern SCS (simplified after Liu, Colin, et al., 2010). Core MD12-3434 in this study and referenced ODP Site 1145 (19°35.04′N, 117°37.86′E, water depth 3,175 m) are located on the lower continental slope with water depths of around 3,000 m, while other referenced Core MD05-2904 (19°27.32′N, 116°15.15′E, water depth 2,066 m), Core MD05-2905 (20°08.17′N, 117°21.61′E, water depth 1,647 m), ODP Site 1144 (20°03.18′N, 117°25.14′E, water depth 2,037 m), and ODP Site 1146 (19°27.40′N, 116°16.27′E, water depth 2,092 m) are located along the mainstream pathway of contour currents with water depths of around 2,000 m. These sediment cores are situated at two depth transects on the slope, that is, T1 including ODP Site 1146, Cores MD05-2904, MD12-3432, and MD12-3434, and T2 including Core MD05-2905, ODP Sites 1144 and 1145. Isobaths of 120, 1,000, 2,000, and 3,000 m are shown by the light-gray lines, respectively. Numbers indicate major surface currents in the northern SCS (black for winter, red for summer): 1, SCS Branch of Kuroshio Current; 2, SCS Warm Current; 3, Coastal Current (Fang et al., 1998).

(e.g., Y. J. Cheng et al., 2016; Y. J. Wang et al., 2001, 2008). As one of the most important archives for paleoclimate and paleoceanography research, deep-sea sediments in the East Asia marginal seas seem to respond selectively to these abrupt climate changes. There are several excellent records of millennial-scale variations of the East Asian monsoon evolution in the Japan Sea that are mainly correlated to the gray scale profile of hemipelagic sediments and the eolian inputs (Nagashima et al., 2007, 2011; Tada, 2004; Tada et al., 1999). Whereas those rapid climate signals preserved in the deep-sea sediments in other low-latitude marginal seas are irregular and/or ambiguous in comparison with all the above records (Chang et al., 2009; Lin et al., 2006, 2014; Oppo & Sun, 2005; L. Wang et al., 1999; Wei et al., 2007; M. X. Zhao et al., 2006). For example, foraminiferal Mg/Ca ratio record of sea surface temperature (SST) during the last glaciation in the low-latitude South China Sea (SCS) indicates clear Heinrich standials with indistinct DO interstandials that are associating with the rapid East Asian monsoon variations (Oppo & Sun, 2005), while $U^{K'}_{37}$ -SST record selectively displays several DO interstandials without obvious Heinrich standials (M. X.Zhao et al., 2006). Consequently, further high-resolution investigations are acquired to better address such problem.

The SCS, as the largest marginal sea in low-latitude monsoonal East Asia, plays a significant role in reconstructing millennial-scale climate changes. Under warm and humid climatic conditions, the surrounding continents and islands of the SCS are characterized by intense weathering, rapid erosion, and well-developed fluvial systems, including several of the world's largest rivers (i.e., the Pearl River, the Red River, and the Mekong River) and numerous small mountainous rivers (e.g., Cho-Shui, Kao-Ping, and Erh-Jen in Taiwan). Then, the total fluvial sediment discharge into the SCS can reach up to 700 Mt/year, making it the largest sediment sink among enclosed or semienclosed marginal seas worldwide (Liu & Stattegger, 2014). Such a huge input of terrigenous sediments has resulted in high accumulation-rate deep-sea sedimentary sequences that are particularly suitable for high-resolution paleoceanographic and paleoclimatic studies (L. Wang & Wang, 1990; Wang, Li, Tian, 2014). Millennial-scale changes associated with the East Asian monsoon have been recognized in SST variations reconstructed from high-resolution $U^{K'}_{37}$ and foraminiferal Mg/Ca ratio in the SCS sediments (Lin et al., 2014; Oppo & Sun, 2005; Wei et al., 2007; M. X. Zhao et al., 2006). These previous studies mainly focus on millennial-scale climate change signals fingerprinted in the biogenic components. However, how these river-borne terrigenous sediments responding to the rapid changes of the East Asian monsoon remains poorly understood (Lin et al., 2006; L. J. Wang et al., 1999; Xie et al., 2014). Moreover, by comparison with rapid climate change records in other low-latitude marginal seas, such as the Caribbean Sea (Peterson et al., 2000; Riboulleau et al., 2014), the Arabian Sea (Deplazes et al., 2013), and marginal area of northwest Africa (Tjallingii et al., 2008), such high accumulation-rate deep-sea sediments in the low-latitude SCS appear to be less sensitive to record the rapid changes of the prevailing East Asian monsoon.

As direct weathering products of continental bedrocks, clay minerals are the most important components of terrigenous sediments, providing one of the most powerful tools for reconstructing the long-term East Asian monsoon evolution in the SCS (Boulay et al., 2005; Chen et al., 2017; Clift et al., 2014; Liu et al., 2003, 2004; Wan et al., 2007). During the typical glacial-interglacial cycles, increase of illite and chlorite contents under reinforced physical erosion is considered to be associated with strengthened winter monsoon, while increase of smectite and kaolinite contents is related to intensive chemical weathering and then indicates strengthened summer monsoon (Liu et al., 2003, 2004). Recently, clay mineralogical records have been demonstrated well displaying the H1 stadial occurred at around 16 ka BP in several northern SCS sediment cores (Liu, Li, et al., 2010, Liu et al., 2016; Huang et al., 2011), implying that clay minerals could be used potentially as an efficient proxy to reflect the millennial-scale climate changes in the East Asian marginal seas. This mineralogical proxy has been realized by high-resolution paleoenvironmental studies in the Cariaco Basin, the Andaman Sea, and the Mediterranean Sea, indicating that clay mineralogy is sensitive enough to respond to interannual- to millennial-scale paleoenvironmental changes, such as interannual paleostorm activity, decadal lunar nodal tidal periodicity (16.8 yr), and millennial Intertropical Convergence Zone (ITCZ) shifts and monsoon variations (Ali et al., 2015; Black et al., 2009; Riboulleau et al., 2014; Sabatier et al., 2010).

In this study, we have investigated the high-resolution clay mineral assemblage combined with Nd and Sr isotopic compositions of sediments from Core MD12-3434 located in the low-latitude northern SCS in order to (1) understand the mechanism of rapid response of terrigenous sediment to the prevailing East Asian monsoon during the last glaciation and (2) to reveal millennial-scale change features of the East Asian monsoon preserved in deep-sea sediments and their potential correlations with high-latitude abrupt climatic changes.

The obtained temporal variations of the clay mineral assemblage indicate distinct millennial-scale changes that are associating with the East Asian summer monsoon evolution, which is realized through contemporaneous chemical weathering and/or sediment supply capacity under strong physical erosion in sedimentary source lands. The study helps to better understand the mechanism of the prompt responses of the low-latitude East Asian monsoon system to abrupt millennial-scale climatic changes occurred in the high-latitude Northern Hemisphere (e.g., Greenland, North Atlantic).

2. Materials and Methods

CASQ Core MD12-3434 (18°49.84′N, 116°18.89′E, water depth 2,995 m) analyzed in this study was collected on the lower continental slope of the northern SCS during the MD190 CIRCEA Cruise in 2012 (Figure 1). The core is 8.33 m long and is dominated by homogenous gray-dark clay without visible bioturbation (Kissel et al., 2012). The age model of this core was established using high-resolution planktonic foraminiferal (*G. ruber*) $\delta^{18}O$ stratigraphy (321 samples) combined with eight AMS ^{14}C dates (X. X. Wang, 2015). These AMS ^{14}C dates were analyzed at the Beta Analytic Laboratory (USA) and were converted to calendar years by using the CALIB 7.0 program, with a 400-year reservoir correction and a Marine13 radiocarbon calibration curve (Reimer et al., 2013). The result shows an age of ~78 ka BP at the bottom (8.33 m) of the core. The average sedimentation rate is 10.68 cm/ka. A total of 415 samples were collected at a 2 cm space through the entire core with an average temporal resolution of 186 years for clay mineralogical analysis. Eight samples from this set were selected in the intervals with distinct clay mineral composition changes for Nd and Sr isotope analysis.

Clay minerals were identified by X-ray diffraction (XRD) using a PANalytical X'Pert PRO diffractometer at the State Key Laboratory of Marine Geology (Tongji University) on oriented mounts of decarbonated clay-sized (<2 μm) particles. The preparation of oriented mounts followed the methods described in details by Liu et al. (2004). Each sample was measured 3 times under conditions of air-drying, ethylene-glycol solvation for 24 hr, and heating at 490°C for 2 hr. Identification and interpretation of clay minerals were made mainly according to the (001) basal reflections on the three XRD diagrams. The proportions of clay minerals were calculated semiquantitatively using the MacDiff software (Petschick, 2000), based on peak areas of basal reflections of smectite (including mixed layers; 15–17 Å), illite (10 Å), and kaolinite/chlorite (7 Å) on the glycolated curve. Relative proportions of kaolinite and chlorite were determined based on the ratio of the 3.57/3.54 Å peak areas. Following the laboratory routine, weighing factors introduced by Biscaye (1965) or Holtzapffel (1985) were not used when generating relative weight percentages of each clay mineral. Replicate analysis of the duplicate oriented mounts of a few selected samples gave a precision of ±2% (2σ). Based upon the XRD method, the semiquantitative evaluation of each clay mineral has an accuracy of ~5%. Additionally, illite crystallinity was obtained from half height width of the 10 Å peak on the glycolated curve.

Nd and Sr isotopic compositions were analyzed on bulk terrigenous (carbonate- and organic-free) sediments using a Thermo Scientific Multi-Collector Induced Coupled Plasma Mass Spectrometer (MC-ICPMS NEPTUNE ^{Plus}) at the Laboratoire des Sciences du Climat et de l'Environnement in Gif-sur-Yvette. In brief, samples were decarbonated by leaching with 20% acetic acid in an ultrasonic bath, and rinsed 5 times and centrifuged to eliminate traces of the carbonate solution. They were then heated at 600°C for 2 hr to remove the organic carbon. Decarbonated and organic-free samples were dissolved in HF-$HClO_4$ and HNO_3-HCl mixtures. A first chemical separation was done using Biorad columns packed with AG50W-X8, 200–400 mesh cation exchange resins. The Sr fraction was purified on a 20 μl Sr-Spec column consisting of a polyethylene syringe with a 4 mm Ø Millex filter (Colin et al., 2014), while Nd was extracted and purified from the REE fraction by using a Ln-Spec column (Copard et al., 2010). The Sr and Nd isotopic compositions were analyzed on MC-ICPMS at a concentration of 15 ppb, and their mass-fractionation correction was done by normalizing $^{86}Sr/^{88}Sr$ to 0.1194 and $^{146}Nd/^{144}Nd$ to 0.7219 and applying an exponential-fractionation correction. Nd results are expressed as $\varepsilon Nd = [(^{143}Nd/^{144}Nd_{meas})/0.512638–1] \times 1000$, using the CHUR value of meteorites as given by Jacobsen and Wasserburg (1980).

3. Results

The clay mineral assemblage of Core MD12-3434 since 78 ka BP consists of dominant smectite (25–50%, average 39%) and illite (25–43%, average 33%), moderate chlorite (17–27%, average 21%), and minor kaolinite (3–12%, average 7%; Figure 2; Supporting Information Table S1). Among the relative content variations of

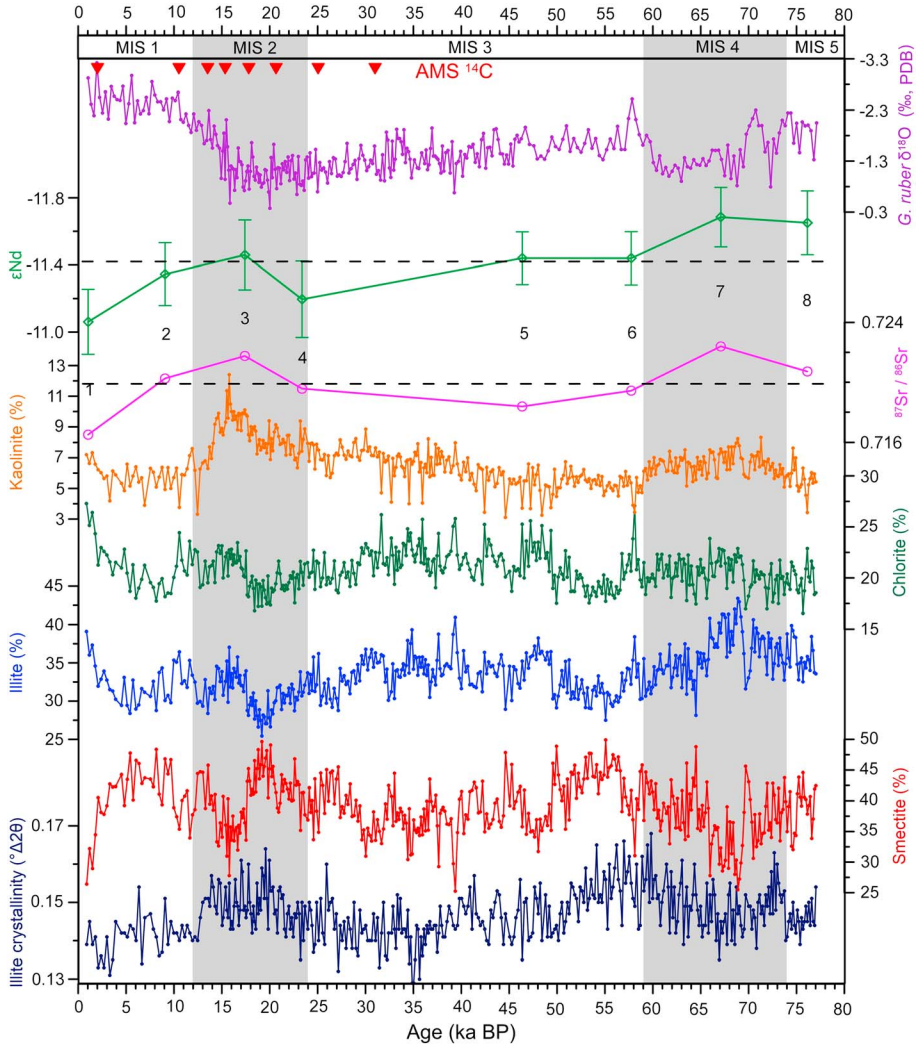

Figure 2. High-resolution clay mineral assemblage of Core MD12-3434. Nd and Sr isotopic compositions of eight samples (with marked numbers of data points following a sequence in Table 1) are presented with their average (dashed lines) and error values. Planktonic foraminiferal $\delta^{18}O$ stratigraphy and AMS ^{14}C dates (red triangles) are from X. X. Wang (2015).

the four clay minerals, illite and chlorite display similar variations, which are inversely correlated to smectite. Temporal variations of these three clay minerals do not show glacial-interglacial cyclicity but display clear millennial-scale changes throughout the complete record. By contrast, kaolinite has a distinct variation pattern with obvious glacial-interglacial change, that is, relatively higher contents during Marine Isotope Stages (MIS) 2 and 4 and lower contents during MIS 1 and 3. Illite crystallinity varies in the range from 0.129 to 0.168 °Δ2θ, and its temporal variation follows the pattern of illite and smectite contents, with lower crystallinity values being accompanied by higher illite content versus lower smectite content.

εNd values and $^{87}Sr/^{86}Sr$ ratios of terrigenous sediments from Core MD12-3434 vary in narrow ranges from −11.7 to −11.1 and from 0.7165 to 0.7224, respectively (Figure 2 and Table 1). Both εNd values and $^{87}Sr/^{86}Sr$ ratios present similar variation patterns with relatively lower εNd values and higher $^{87}Sr/^{86}Sr$ ratios during MIS 2 and 4, and higher εNd values and lower $^{87}Sr/^{86}Sr$ ratios during MIS 1 and 3.

4. Discussion

4.1. Sources and Transport Processes of Clay Minerals

To understand the paleoenvironmental implications of millennial-scale clay mineralogical variations at Core MD12-3434, the key issue is the knowledge of sediment sources and their transport processes. Previous

Table 1
Nd and Sr Isotopic Compositions of Core MD12-3434 and Referenced Sediment Cores and Their Three End-Member Provenances Surrounding the Northern SCS

No.	Sample	Latitude (°N)	Longitude (°E)	$^{87}Sr/^{86}Sr$	±2δ	$^{143}Nd/^{144}Nd$	±2δ	εNd (±2δ)
MD12-3434		18.831	116.315					
1	0 cm			0.716495	0.000010	0.512071	0.000010	−11.06 ± 0.19
2	54 cm			0.720259	0.000011	0.512056	0.000010	−11.35 ± 0.19
3	140 cm			0.721756	0.000011	0.512051	0.000011	−11.46 ± 0.21
4	226 cm			0.719576	0.000014	0.512064	0.000012	−11.20 ± 0.23
5	470 cm			0.718381	0.000010	0.512052	0.000008	−11.44 ± 0.16
6	588 cm			0.719433	0.000010	0.512052	0.000008	−11.44 ± 0.16
7	700 cm			0.722403	0.000010	0.512039	0.000009	−11.68 ± 0.18
8	816 cm			0.720717	0.000011	0.512041	0.000010	−11.65 ± 0.19
MD05-2905		20.136	117.36	(Data source: Liu ZF, unpublished data)				
9	0 cm			0.718437	0.000011	0.512058	0.000008	−11.31 ± 0.16
10	190 cm			0.718890	0.000013	0.512057	0.000010	−11.34 ± 0.20
11	382 cm			0.721043	0.000011	0.512052	0.000007	−11.44 ± 0.15
12	564 cm			0.719197	0.000012	0.512052	0.000008	−11.44 ± 0.15
13	682 cm			0.719678	0.000012	0.512034	0.000009	−11.78 ± 0.18
14	760 cm			0.720010	0.000010	0.512037	0.000009	−11.72 ± 0.17
15	918 cm			0.718951	0.000012	0.512040	0.000012	−11.67 ± 0.24
16	1,016 cm			0.718783	0.000010	0.512054	0.000008	−11.40 ± 0.16
17	1,116 cm			0.719053	0.000010	0.512055	0.000007	−11.37 ± 0.13
ODP Site 1145		19.584	117.631	(Data source: Boulay et al., 2005)				
18	88 cm			0.71633	0.00001	0.512099	0.000007	−10.51 ± 0.14
19	158 cm			0.71698	0.00002	0.512080	0.000008	−10.88 ± 0.16
20	338 cm			0.71912	0.00001	0.512067	0.000009	−11.14 ± 0.18
21	478 cm			0.71654	0.00001	0.512082	0.000008	−10.85 ± 0.16
22	858 cm			0.71786	0.00001	0.512069	0.000006	−11.10 ± 0.12
23	978 cm			0.71487	0.00003	0.512105	0.000008	−10.40 ± 0.16
24	1,298 cm			0.72122	0.00001	0.512050	0.000006	−11.47 ± 0.12
25	1,438 cm			0.71831	0.00001	0.512083	0.000006	−10.83 ± 0.12
26	1,538 cm			0.72227	0.00001	0.512064	0.000008	−11.20 ± 0.16
27	1,738 cm			0.71900	0.00001	0.512085	0.000007	−10.79 ± 0.14
Pearl River (surface sediments; data source: Liu et al., 2007)								
28	PR04	23.110	113.896	0.733442	0.000003	0.512039	0.000041	−11.68 ± 0.80
29	PR09-2	24.180	113.422	0.742222	0.000005	0.511957	0.000006	−13.28 ± 0.12
30	PR15-2	23.151	112.891	0.735662	0.000006	0.511989	0.000005	−12.66 ± 0.10
31	PR19	23.172	112.346	0.735209	0.000003	0.512106	0.000009	−10.38 ± 0.18
32	PR25	23.456	111.480	0.727507	0.000002	0.512004	0.000003	−12.37 ± 0.06
33	PR30	23.423	110.536	0.730134	0.000003	0.512053	0.000009	−11.41 ± 0.18
34	PR37-2	24.317	109.468	0.737314	0.000005	0.512099	0.000029	−10.51 ± 0.57
35	PR40-1	22.681	109.260	0.728329	0.000002	0.512025	0.000003	−11.96 ± 0.06
Luzon rivers (surface sediments; Data source: Liu et al., 2016)								
36	LZ03	14.939	120.761	0.704391	0.000010	0.513001	0.000007	7.08 ± 0.14
37	LZ13	15.980	120.226	0.704801	0.000011	0.512998	0.000009	7.02 ± 0.17
38	LZ22	17.559	120.467	0.704198	0.000029	0.513017	0.000008	7.39 ± 0.15
39	LZ31	18.123	121.673	0.704608	0.000011	0.513002	0.000008	7.10 ± 0.16
40	LZ36	16.972	121.657	0.704896	0.000029	0.513006	0.000009	7.19 ± 0.17
Taiwan rivers (surface sediments; data source: Liu et al., 2016)								
41	CK2	23.836	120.284	0.718828	0.000010	0.512032	0.000007	−11.83 ± 0.14
42	CK5	23.085	120.127	0.721323	0.000012	0.512010	0.000009	−12.24 ± 0.17
43	CK6	22.918	120.185	0.720608	0.000011	0.511991	0.000009	−12.63 ± 0.18
44	CK7-1	22.637	120.442	0.718899	0.000029	0.512043	0.000007	−11.60 ± 0.14
45	CK10	22.794	121.139	0.715471	0.000029	0.512065	0.000007	−11.19 ± 0.13

studies on clay mineralogical and geochemical compositions of widespread seafloor and surrounding fluvial sediments have indicated that northern SCS terrigenous sediments are mainly derived from fluvial systems of three end-member sources, that is, South China (mainly the Pearl River), Taiwan, and Luzon (Liu, Colin, et al., 2010, 2016), while eolian input is considered as insignificant (e.g., Boulay et al., 2005; Liu et al., 2003, Liu, Li, et al., 2010; Wan et al., 2007). Clay mineral assemblages that these three end-member sources provide are distinct. South China provides dominant kaolinite (30–67%) with moderate illite (6–40%) and chlorite

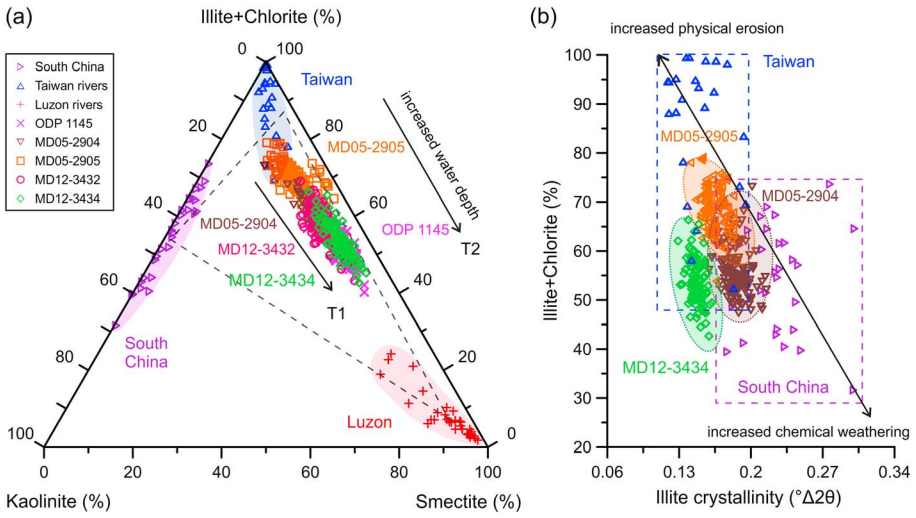

Figure 3. (a) Ternary diagram of major clay groups (illite + chlorite, kaolinite, and smectite) of Core MD12-3434. The dotted lines indicate the mixing curves between the three end-members. Clay mineral values of three end-member provenance (South China, Taiwan, and Luzon) and neighboring referenced sediment cores along transects T1 and T2 are also displayed for comparison. (b) Illite + chlorite versus illite crystallinity diagram of Core MD12-3434 and its comparison with that of Taiwan and South China sources. Data of South China (the Pearl River) from Liu et al. (2007), data of Taiwan rivers from Liu et al. (2008), data of Luzon rivers from Liu et al. (2009), data of ODP Site 1145 from Boulay et al. (2005), data of Core MD05-2904 from Liu, Li, et al., 2010; Liu et al., 2016), data of Core MD05-2905 from Liu ZF (unpublished data), and data of Core MD12-3432 from Chen et al. (2017).

(15–37%), Luzon provides dominant smectite (60–97%), whereas Taiwan provides dominant illite (44–66%) and chlorite (33–48%; Liu et al., 2007, 2008, 2009). Moreover, it has been convinced that lithological and geomorphologic settings, rather than climatic conditions, are the major controlling factors on clay mineral production in the three-end member source regions (see detail discussion in Liu et al., 2016). Consequently, these three end-member sources have provided quite similar clay mineral assemblages to the SCS since the Late Quaternary as those of today, that is, major kaolinite from South China, illite and chlorite from both South China and Taiwan, and principal smectite from Luzon (Chen et al., 2017; Liu, Colin, et al., 2010; Liu et al., 2016).

However, Hu et al. (2013) argued that the clay mineral assemblage provided by the Pearl River system could change during the Holocene and then is not suitable for provenance analysis during the geological past. Such interpretation is based on a sediment core record of high smectite contents (~35%) at 2.5 ka BP nearby Hong Kong in the Pearl River mouth region. In consideration of the widespread granitic and sedimentary rocks versus the limited distribution of volcanic rocks in the Pearl River drainage basin, the long-term intensive chemical weathering along with flat topography only permits the formation of large amounts of kaolinite, instead of smectite (Liu et al., 2007, Liu, Colin, et al., 2010). The high content of smectite observed by Hu et al. (2013) should be very locally distributed and mostly derived from small neighboring volcanic islands and/or transported by coastal currents from nearby bays (Liu et al., 2014). Therefore, we believe that the modern clay mineral assemblages provided by the three end-member sources remain appropriate references for sediment source analysis (Chen et al., 2017; Liu, Colin, et al., 2010, Liu, Li, et al., 2010; Liu et al., 2016).

A ternary diagram reporting the proportion of illite + chlorite, kaolinite, and smectite indicates that the dominant clay minerals of Core MD12-3434 have been provided mainly by Taiwan and Luzon, with a minor proportion of South China (Figure 3a). It is evidenced by the observation that all the clay mineral data of Core MD12-3434 plot linearly between Taiwan and Luzon sources, with a slight shift to the South China source in the ternary diagram. Additionally, low values of illite crystallinity (0.129–0.168°Δ2θ) of Core MD12-3434 (Figure 2) are within the variation range of Taiwan-sourced illite crystallinity (0.120–0.211°Δ2θ; Liu et al., 2008), while are much lower than that of the South China-sourced illite (0.159–0.301°Δ2θ; Liu et al., 2007; Figure 3b), implying that Taiwan is the predominant source of illite. Because the analogous illite and chlorite usually have the same sources for sediments in the northern SCS (Liu, Colin, et al., 2010; Liu et al., 2016), it can be concluded that Taiwan is the major source of illite and chlorite for Core MD12-3434. Furthermore, in view of limited South China-sourced illite and chlorite, the low value of kaolinite (~7%) of Core MD12-3434 that is

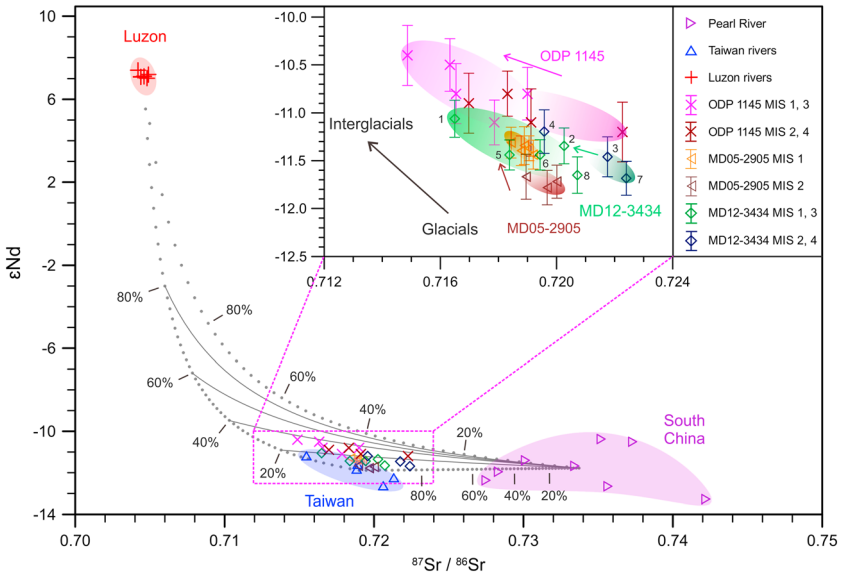

Figure 4. Variations of εNd value versus $^{87}Sr/^{86}Sr$ ratio of Core MD12-3434 compared with terrigenous provenance end-members (South China, Taiwan, and Luzon). Data of referenced Core MD05-2905 and ODP Site1145 are also included. The dotted grey lines indicate the mixing curves between the three end-members. The inset plot shows variations of the samples between glacial (cold) and interglacial (warm) periods from these three sediment cores. Numbers indicate Nd and Sr isotopic data points of Core MD12-3434 following a sequence in Table 1. Data of South China (the Pearl River) from Liu et al. (2007), data of Taiwan and Luzon from Liu et al. (2016), data of ODP Site1145 from Boulay et al. (2005), and data of Core MD05-2905 from Liu ZF (unpublished data). See Table 1 for detailed Sr and Nd isotopic compositions.

just comparable to the background value (~5%) of deep basin (Liu et al., 2016) indicates a less clay contribution from South China. This result is further well correlated to an estimation of clay contributions of Core MD12-3434 from each end-member source region. Using a linear separation method for illite crystallinity designed by Liu et al. (2008) and (Liu, Li, et al., 2010), the clay contributions of Core MD12-3434 have 39–67% (average 54%) from Taiwan, 23–53% (average 39%) from Luzon, and 3–15% (average 7%) from South China for the past 78 ka (unpublished data).

Nd and Sr isotopes of bulk terrigenous sediments of Core MD12-3434 fall in the field delimited by the mixing curves between South China, Taiwan rivers, and Luzon rivers, also suggesting the same three end-member sources (Liu et al., 2007, 2016; Figure 4). As εNd values and $^{87}Sr/^{86}Sr$ ratios plot nearby the end-member corresponding to the Taiwan rivers' isotopic compositions while far from South China and Luzon, it can be concluded that bulk terrigenous sediments of Core MD12-3434 are mainly derived from Taiwan with a minor contribution from South China and Luzon. Such observation is further confirmed by semiquantitative calculation, presenting that bulk terrigenous sediment contributions from Taiwan, Luzon, and South China are 70–85% (average 77%), 5–20% (average 15%), and 5–15% (average 8%), respectively (Figure 4). The result based on bulk Nd and Sr isotopes is mostly in agreement with the source analysis from the clay mineralogy (Figure 3). However, there is slight difference between Luzon-sourced bulk and clay sediments, and we believe that the difference is due to the different grain size groups of terrigenous sediments that are quantitatively calculated. To sum up, terrigenous sediments of Core MD12-3434 are mainly derived from Taiwan, while Luzon and South China provide moderate and minor proportions, respectively.

Temporal variations of Nd and Sr isotopes have indicated that terrigenous sediment sources of Core MD12-3434 present clear glacial-interglacial cyclicity during the past 78 ka (Figure 4). For glacial sediments (MIS 2 and 4), lower εNd values and higher $^{87}Sr/^{86}Sr$ ratios imply a higher contribution of sediments provided by Taiwan and/or South China. Considering the synchronously increased terrigenous fluxes at Core MD12-3434 (S. H. Zhao et al., 2017), this higher sediment contribution has indeed indicated the significant increased terrigenous fluxes from Taiwan and limited increased terrigenous fluxes from South China because of its overall minor contribution. In contrast, for interglacial sediments of Core MD12-3434 (MIS 1 and 3), higher εNd values and lower $^{87}Sr/^{86}Sr$ ratios suggest a higher contribution of sediments deriving from Luzon, the

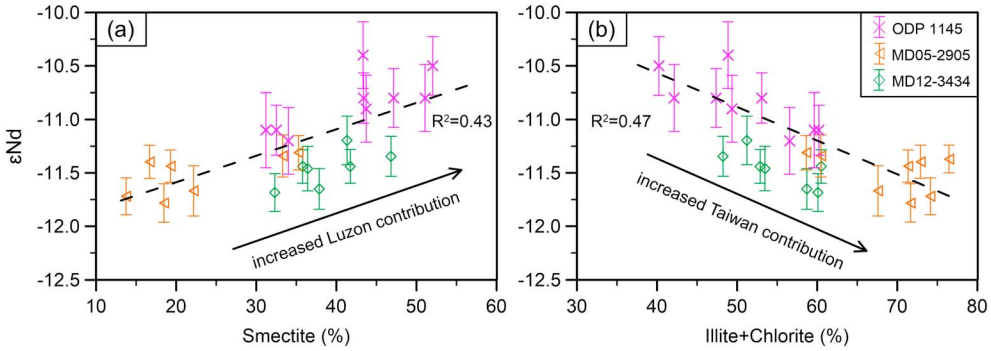

Figure 5. Linear correlation of εNd with clay mineral compositions of Core MD12-3434 compared with referenced Core MD05-2905 and ODP Site1145. (a) εNd versus smectite (%); (b) εNd versus illite + chlorite (%). The dashed lines indicate correlations with a coefficient of R^2. Data of ODP Site1145 from Boulay et al. (2005) and data of Core MD05-2905 from Liu ZF (unpublished data).

value of which was estimated to be ~17% using the same semiquantitative calculation method as above. Being further in combination with the average value of terrigenous fluxes (4.48 g · cm^{-2} · ka^{-1}) at Core MD12-3434 (S. H. Zhao et al., 2017), the averaged terrigenous flux from Luzon during interglacials is estimated to be 0.76 g · cm^{-2} · ka^{-1}. Similarly, the averaged terrigenous flux from Luzon during glacials is estimated to be 0.54 g · cm^{-2} · ka^{-1} (an average contribution of 10% from Luzon versus an average terrigenous flux of 5.36 g · cm^{-2} · ka^{-1}; S. H. Zhao et al., 2017). Obviously, the terrigenous fluxes from Luzon during interglacials are higher than that during glacials, confirming that a higher sediment contribution sourced from Luzon inferred from higher εNd values and lower $^{87}Sr/^{86}Sr$ ratios also implies an increased terrigenous fluxes. Moreover, such glacial-interglacial variations of the Nd and Sr isotopic compositions are also observed in sediments of the adjacent ODP Site 1145 (Boulay et al., 2005) and Core MD05–2905 (Liu Z. F., unpublished data; Figure 4).

Simultaneously, linear correlations are observed between terrigenous εNd values and smectite % (R^2 = 0.43) as well as illite + chlorite % (R^2 = 0.47) for Core MD12-3434, Core MD05-2905, and ODP Site 1145 (Boulay et al., 2005; Liu Z. F., unpublished data; Figure 5). These correlations provide new evidences for millennial-scale variations of sedimentary sources in the northern SCS. An increase of smectite content is always associated with a significant increase of the εNd values of Core MD12-3434, suggesting a relatively increased contribution of clayey sediments deriving from Luzon (Figure 5a), further implying increased clay fluxes from Luzon. By contrast, an increase of illite and chlorite contents is associated with a decrease of the εNd values, implying a relatively increased contribution of more clayey sediments provided by Taiwan (Figure 5b), that is, increased clay fluxes from Taiwan. Therefore, the rapid changes of smectite and illite and chlorite of Core MD12-3434 have certainly indicated the millennial-scale source variations of clayey sediments, mainly between two end-member sources: Luzon and Taiwan.

Terrigenous sediments from the three end-member sources are transported by different oceanic currents to the northern SCS (Liu, Colin, et al., 2010; Liu et al., 2016; Zhong et al., 2017; Figure 1b). South China-sourced sediments are predominantly transported by the westward coastal currents. In particular, owing to differential settling and/or flocculation, the relatively coarser-grained kaolinite from South China flocculates and settles fast when encountering the alkaline seawater (Liu et al., 2016; Schroeder et al., 2015). Then, predominate South China-sourced kaolinite is further trapped in a confined area west of the Pearl River mouth and is hardly transported into the abyssal basin. Luzon-sourced sediments (principal fine-grained smectite) are carried mainly by the westward surface currents with significant influence of the Kuroshio intrusion through a long transport distance (Liu, Colin, et al., 2010). Taiwan-sourced sediments (predominant illite and chlorite) are mostly delivered by deep-water currents to the deep basin (mainly contour currents; Liu, Colin, et al., 2010; Y. L. Zhao et al., 2015). During the glacial periods (MIS 2 and 4), the drop of sea levels led to the seaward migration of the paleo-river mouth, causing more South China-sourced terrigenous sediments to be transported to the area of Core MD12-3434 (S. H. Zhao et al., 2017). This mechanism could explain the slight increase of kaolinite during the glacial periods (from MIS 4 to MIS 2; Figure 2). Nevertheless, the low kaolinite content (average 7%) of Core MD12-3434 throughout the entire record indicates that the influence of such

mechanism is not an important factor affecting the clay mineral assemblage variations. Luzon-sourced smectite and Taiwan-sourced illite and chlorite are the most significant for temporal variations of clayey sediments at Core MD12-3434 during the glacial periods.

To summarize, our results show that clay minerals of Core MD12-3434 are mainly derived from fluvial sediments of Taiwan and Luzon, with a minor contribution of South China (mainly the Pearl River). Taiwan contributes mostly illite and chlorite, while Luzon and South China contribute smectite and kaolinite, respectively. Illite and chlorite from Taiwan are transported to the northern SCS via the deep contour currents, while smectite from Luzon is transported mostly by the westward surface currents.

4.2. Clay Mineralogical Proxy of the East Asian Summer Monsoon Evolution and the Potential Influence by Oceanic Currents

According to the sediment source analysis discussed above, temporal variations of clay minerals at Core MD12-3434 during the last glaciation are largely due to the proportion of Luzon-sourced smectite to Taiwan-sourced illite and chlorite. Multiproxy studies of source-to-sink transport processes of the SCS sediments have indicated that the clay mineral variations in the source areas are strongly associated the prevailing East Asian summer monsoon, and upon entering the SCS (Liu et al., 2007, 2008, 2009), they are further impacted by different oceanic currents (Liu, Colin, et al., 2010; Liu et al., 2016; Zhong et al., 2017). Consequently, the possible mechanisms that driving the temporal variations of clay minerals at Core MD12-3434 can be correlated to (1) the East Asia summer monsoon changes and/or (2) oceanic current intensifications including the surface current which transporting Luzon-sourced smectite and contour current that carrying Taiwan-sourced illite and chlorite.

4.2.1. Clay Mineral Variations Associating With the East Asian Summer Monsoon Intensity

Clay mineral formation in both Luzon and Taiwan is strongly controlled by high temperature and strong rainfall under the prevailing East Asian summer monsoon (Liu et al., 2008, 2009). Then, the temporal variations of clay minerals of Core MD12-3434 derived from these two sources can be probably attributed to the East Asian summer monsoon changes. This linkage can be realized through changes in (1) clay mineral formation rate that is associated with chemical weathering and physical erosion intensity variations of bedrocks and/or (2) clay mineral supply capacity correlated with fluvial systems that are controlled by monsoonal rainfall. It must be pointed out that the definition of the East Asian summer monsoon intensity is still under debate (B. Wang, Wu, et al., 2008). Normally, the rainfall strength change characterized by a seasonal north-south migration could be used as the main indicator for the East Asian summer monsoon intensity. This concept was first proposed by B. Wang, Wu, et al. (2008) and further affirmed by Wang, Wang, et al., (2014) P. X. Wang et al. (2017). In this study, we adopt this definition to better understand the East Asian summer monsoon variations during the last glaciation, due to its more proper interpretation for the clay mineral changes.

Luzon-sourced smectite is produced from volcanic rocks through the rapid chemical weathering process associated with strong physical erosion under strong monsoon rainfall (Liu et al., 2009). The prevailing subtropical East Asian monsoon climate (warm and humid) with an active tectonic setting in Luzon has led to an ever known higher rate of chemical weathering in the tropics (114–396 $g \cdot m^{-2} \cdot yr^{-1}$; Schopka et al., 2011). Widespread andesitic-basaltic volcanic rocks thereby are always suffered from the strong chemical weathering processes that allow the rapid production of large amounts of smectite with good crystallinity (Liu et al., 2009). Due to the heavy monsoonal rainfall with strong physical erosion intensity, smectite is washed away from rock surfaces shortly after its formation, preventing it from continuous chemical weathering toward halloysite and kaolinite. This result is supported by the moderate-intensive weathering degree of river surface clay sediments in Luzon, inferred from the chemical index of alteration values of 75–90 (Liu et al., 2009). In particular, recent studies have demonstrated that chemical weathering rate can respond rapidly to decade- to millennial-scale climate changes with rainfall and temperature variations (e.g., Beaulieu et al., 2012; Dosseto et al., 2015; Gislason et al., 2009). Then, the increased East Asian summer monsoon dominates variations of rainfall and temperature that can contemporaneously increase the chemical weathering rate in Luzon during various timescale, resulting in more smectite formation and transportation to the SCS. Synchronously, the intensified monsoonal rainfall is also in favor of strengthened sediment loading capacity of these small rivers in Luzon, and then leads to enhanced terrigenous fluxes from Luzon to the SCS and increased smectite content in the deep-sea sediments. Therefore, the increase in smectite content sourced from Luzon potentially stands for the strengthened East Asian summer monsoon.

In contrast, Taiwan-sourced illite and chlorite are produced from reinforced physical erosion of bedrocks (Liu et al., 2008). Taiwan is strongly influenced by active tectonic settings along with strong typhoon/monsoonal rainfall, resulting in reinforced physical denudation characterized by extremely high erosion rates of 3–6 mm/year (Dadson et al., 2003; Hartshorn et al., 2002). In this case, widespread sedimentary and metamorphic rocks in high mountains of Taiwan always produce large amounts of illite and chlorite (Liu et al., 2008). These weathering products are then efficiently cleared by seasonal runoff shortly after their formation, instead of being further weathered chemically (Hartshorn et al., 2002). As a result, the illite usually has good crystallinity (low value) and low chemical index that both stand for a moderate degree of weathering (Liu et al., 2008; Figure 3b). The mineralogical features are in agreement with a moderate chemical index of alteration values (76–86) of fluvial clayey sediments (Liu et al., 2016; Selvaraj & Chen, 2006). During the prevailing cold and dry climate like the intervals of YD, Heinrich stadials, and glacial periods associated with the retreat of the East Asian summer monsoon (Sun et al., 2012; Y. J. Wang et al., 2001; Wen et al., 2016), both Taiwan and Luzon tend to exhibit a clear synchronous decrease in rainfall and temperature inferred from a compilation of multiproxy data coupling with model simulations (Ding et al., 2016; Partin et al., 2015). Then, surface processes favor reinforced physical erosion at Taiwan but potentially restrain the chemical weathering at Luzon under relative weakened rainfall intensity (Chen et al., 2017). This leads to reinforced illite and chlorite production in Taiwan while subdued smectite formation and/or smectite supply from Luzon, resulting in decreased smectite fluxes to the SCS. Consequently, decrease of Luzon-sourced smectite companied by increased Taiwan-sourced illite and chlorite of Core MD12-3434 indicates the relatively decreased East Asian summer monsoon intensity (Figure 2).

Accordingly, the formation process and/or supply capacity of clay minerals in both Luzon and Taiwan are contemporaneous to respond to the East Asian summer monsoon variation. Variations of Luzon-sourced smectite versus Taiwan-sourced illite and chlorite at Core MD12-3434 potentially indicate the relatively increase or decrease of the East Asian summer monsoon intensity, associating changes in both the chemical and physical weathering and/or sediment supply capacity. Higher Luzon-sourced smectite contents with lower Taiwan-sourced illite and chlorite contents, which indicate increased clay fluxes from Luzon, suggest the strengthened East Asian summer monsoon, and vice versa. As a result, the smectite/(illite + chlorite) ratio represents the relative proportion of clay minerals deriving from Luzon (smectite) and Taiwan (illite and chlorite) and can be adopted as the mineralogical proxy for establishing the East Asian summer monsoon evolution history. This clay mineralogical ratio, with advantage of eliminating the dilution effects, has been confirmed in several previous studies at the relatively longer timescales (e.g., Boulay et al., 2005; Chen et al., 2017; Liu et al., 2003; Yu et al., 2016).

4.2.2. Influence of Oceanic Currents on Climatic Signals Preserved in Clay Mineralogy

However, in view of the entire source-to-sink transport processes of clay minerals in the northern SCS (Liu, Colin, et al., 2010; Liu et al., 2016), these climate change signals preserved in the clay mineralogical ratio in deep-sea sediments could be further potentially disturbed by oceanic currents, but only with possible limited influence. Westward paleo-surface current, which transported smectite from Luzon, is lack of suitable and comparable evolution records during the last glaciation at present. In view of the close correlation between surface current circulation and monsoon wind direction inferred from modern observations and model simulations (Fang et al., 1998; Hu et al., 2000 and references therein; Figure 1b), the westward surface current is possibly increased during strong summer monsoon periods because of the strengthened wind intensity (L. J. Wang & Wang, 1990; Wang, Li, Tian, 2014). As a result, more smectite transported from Luzon to Core MD12-3434 can lead to an increase in smectite/(illite + chlorite) ratio, tending to enlarge the signals of strengthened summer monsoon. Obviously, this part of increased clay mineralogical ratios associated with the strengthened surface current remains the outcome of strengthened summer monsoon. Meanwhile, Kuroshio intrusion into the modern SCS, which also plays a significant role in transporting Luzon-sourced smectite (Liu, Colin, et al., 2010, 2016), tends to enhance during a period of intense winter monsoon on both interannual and decadal timescales deduced from modern observation data coupling with model simulations (e.g., Hsin et al., 2012; Wu et al., 2017; Wu & Hsin, 2012). Such an observation indicates this proportion of increased Luzon-sourced smectite correlated with the strengthened Kuroshio intrusion could potentially lead to an increase of smectite/(illite + chlorite) ratio during strong winter monsoon periods. However, in contrast to large fluvial sediment fluxes to the SCS during a strong summer monsoon rainfall (e.g., Dadson et al., 2003; Hartshorn et al., 2002; Liu et al., 2009), the increased Luzon-sourced smectite associated with the

strengthened Kuroshio intrusion in winter should only has very limited influence on the variations of clay mineralogical ratio. Therefore, the increased Luzon-sourced smectite at MD12-3434 remains to indicate strengthened summer monsoon signal, though disturbed by the westward surface current with significant influence of the Kuroshio intrusion.

Simultaneously, contour currents that transport illite and chlorite from Taiwan have some influence on the climatic change signals fingerprinted in clay minerals. As an outcome of the North Pacific Deep Water intrusion to the SCS through Luzon Strait, the contour currents characterized by a tunnel-like vertical structure flow along the continental slope at water depth of around 1,650–2,000 m inferred from modern in situ observations (W. Zhao et al., 2014; Y. L. Zhao et al., 2015, and references therein; Figure 1b). Previous studies of the SCS sediments have demonstrated that contour currents is strengthened during Heinrich stadials deduced from the striking increase of both magnetic susceptibility and mean size of sortable silt (Li et al., 2017; Zheng et al., 2016), coinciding with a period of the weakened East Asian summer monsoon (Sun et al., 2012; Y. J. Wang et al., 2001; Wen et al., 2016). Then, the intensified deep contour currents have potentially resulted in more illite and chlorite derived from Taiwan to Core MD12-3434, decreasing the smectite/(illite + chlorite) ratio and tending to amplify the signals of weakened summer monsoon to an unclear certain degree. To further address this problem, results of the present study have been compared with several previous available clay mineralogical records in the northern margin of the SCS (Boulay et al., 2005; Chen et al., 2017; Liu, Li, et al., 2010; Liu et al., 2016; Figures 1b and 3). These clay mineralogical data from several deep-sea sediment cores located along two depth transects on the slope, that is, transect T1 including Cores MD05-2904, MD12-3432, and MD12-3434, while transect T2 including Core MD05-2905 and ODP Site 1145.

Following each transect with increasing water depth (Figure 3a), increased Luzon-sourced smectite versus decreased Taiwan-sourced illite and chlorite can be attributed to relatively calm sedimentary environment that are mainly correlated to the weakened contour currents. Clay minerals of all these sediment cores have been demonstrated to be also provided by the same three-end member sources (Chen et al., 2017; Liu, Li, et al., 2010; Liu et al., 2016), as shown in Figure 3a. Three Cores MD05-2904, MD05-2905, and MD12-3432 (water depths ~2,000 m) on both transects T1 and T2 are situated close to the mainstream pathway of contour currents based on the integrated mooring in situ observation (Y. L. Zhao et al., 2015). All of them receive more Taiwan-sourced illite and chlorite with relatively less Luzon-sourced smectite. By contrast, Core MD12-3434 and ODP Site 1145 (water depths ~3,000 m) are located at the lower part of the slope on the two transects where are beyond the mainstream pathway of contour currents (Y. L. Zhao et al., 2015). The weakened activities of contour currents tend to result in a relatively calm sedimentary environment that permits these two cores to obtain higher contents of fine-grained Luzon-sourced smectite (both at ~39%) than the above three relatively shallow water sites (~34%, ~34%, and ~23% at Cores MD05-2904, MD12-3432, and MD05-2905, respectively). Therefore, as an indicator of contemporaneous chemical weathering and/or terrigenous supply under summer monsoon in Luzon, the high smectite contents of relatively deeper water cores indicate that the deep-sea sediments of the relatively calm sedimentary environments favor to better document these climatic change signals. According to the above discussion, although it is hard to precisely identify the influence from contour currents at this very moment, the clay mineralogical ratio in deep-sea sediments remains to be a powerful proxy to reconstruct the East Asian summer monsoon variations. And importantly, a further comparison of this clay mineralogical ratio between different sediment cores that are located on the same two transects will be conducted to better address this problem related with contour currents in the next section.

4.3. Millennial-Scale Variations of the East Asian Summer Monsoon

The smectite/(illite + chlorite) ratio of Core MD12-3434 has displayed a large range from 0.38 to 1.16 (±0.05–0.16, average ± 0.09, 2σ) with clear millennial-scale changes, providing an excellent record of the millennial-scale East Asian summer monsoon evolutional history (Figure 6). During the last glaciation, rapid increase in smectite/(illite + chlorite) ratio implies that the strengthened East Asian summer monsoon rainfall that is well aligned with the DO and BA interstadials preserved in $\delta^{18}O$ variations of high-latitude Greenland ice cores (North Greenland Ice Core Project [NGRIP] Members, 2004; Figure 6). In contrast, rapid decrease in smectite/(illite + chlorite) ratio suggests the relatively weakened East Asian summer monsoon, coinciding with the H1–H6 and YD stadials. These millennial-scale oscillations of smectite/(illite + chlorite) ratio have

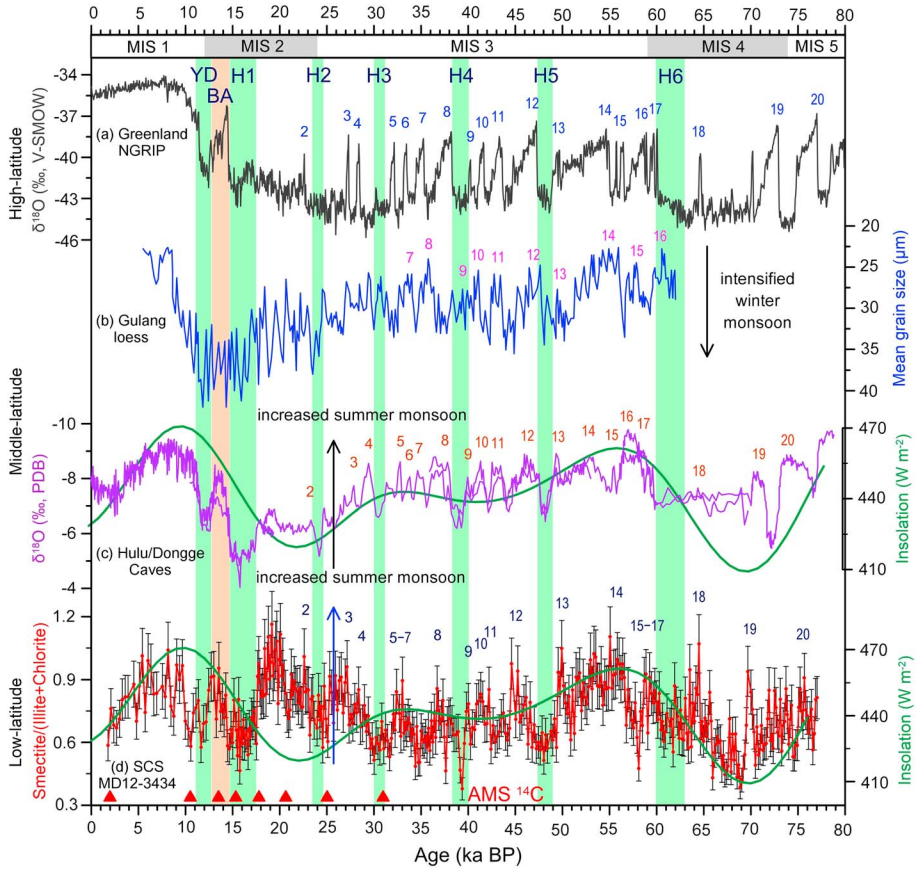

Figure 6. Millennial-scale variations in the smectite/(illite + chlorite) ratio with error (±2σ) of Core MD12-3434 in the low-latitude SCS and their comparison with mean grain size of Gulang loess and $\delta^{18}O$ of Hulu-Dongge cave stalagmites and Greenland NGRIP ice cores. (a) $\delta^{18}O$ record of ice cores from Greenland (NGRIP Members, 2004); (b) mean grain size of Gulang loess profiles (Sun et al., 2012); (c) stalagmite $\delta^{18}O$ records in the Hulu and Dongge Caves (Dykoski et al., 2005; Y.J. Wang et al., 2001) and correlated 21 July insolation at 65° N (green curve; Berger, 1978); (d) smectite/(illite + chlorite) ratio of Core MD12-3434 with AMS ^{14}C dates (red triangles) and correlated 21 July insolation at 65° N (green curve; Berger, 1978). H1–6, YD, BA, and DO events are marked after Y. J. Wang et al. (2001).

indicated that rapid responses of terrigenous sediments in the low-latitude SCS to the prevailing East Asian monsoon are realized mainly through changing contemporaneous chemical weathering rate and/or sediment supply under strong physical erosion from Luzon.

The millennial-scale variations in smectite/(illite + chlorite) ratio of Core MD12-3434 during the last glaciation are also mostly consistent with other East Asian paleomonsoon records, including stalagmite $\delta^{18}O$ of Hulu and Dongge caves (Dykoski et al., 2005; Y.J. Wang et al., 2001) and grain size of Gulang loess (Sun et al., 2012; Figure 6). In combination with the $\delta^{18}O$ records of Greenland ice cores (NGRIP Members, 2004; Figure 6), the distinct synchronicity of the most YD, Heinrich stadials, and BA, DO interstadials fingerprinted by these four differentrecords implies that the punctuated millennial-scale climate changes coevolve from the high-latitude Northern Hemisphere to the middle- and low-latitude East Asian monsoon region. Such a consistency is also confirmed by the similar rapid cyclic variations of Core MD12-3434 smectite/(illite + chlorite) ratio and $\delta^{18}O$ records of Hulu and Dongge cave stalagmites and Greenland ice cores. Both spectral analysis and continuous wavelet on the smectite/(illite + chlorite) ratio reveal a strong periodicity of 4.5 ka and relatively weak high-frequency periodicities of 1.5 and 1.3 ka, which are also comparable to $\delta^{18}O$ records of Hulu and Dongge cave stalagmites and the Greenland ice cores (NGRIP Members, 2004; Wang et al., 2008; Figures 7a and 7b). Their similar cyclicities are further demonstrated by significant spectral power of around 4.5, 1.5, and 1.3 ka bands of the cross wavelet analyses for our clay mineralogical ratio against $\delta^{18}O$ records of the Hulu and Dongge cave stalagmites (Figure 7c) and the Greenland ice cores (Figure 7d).

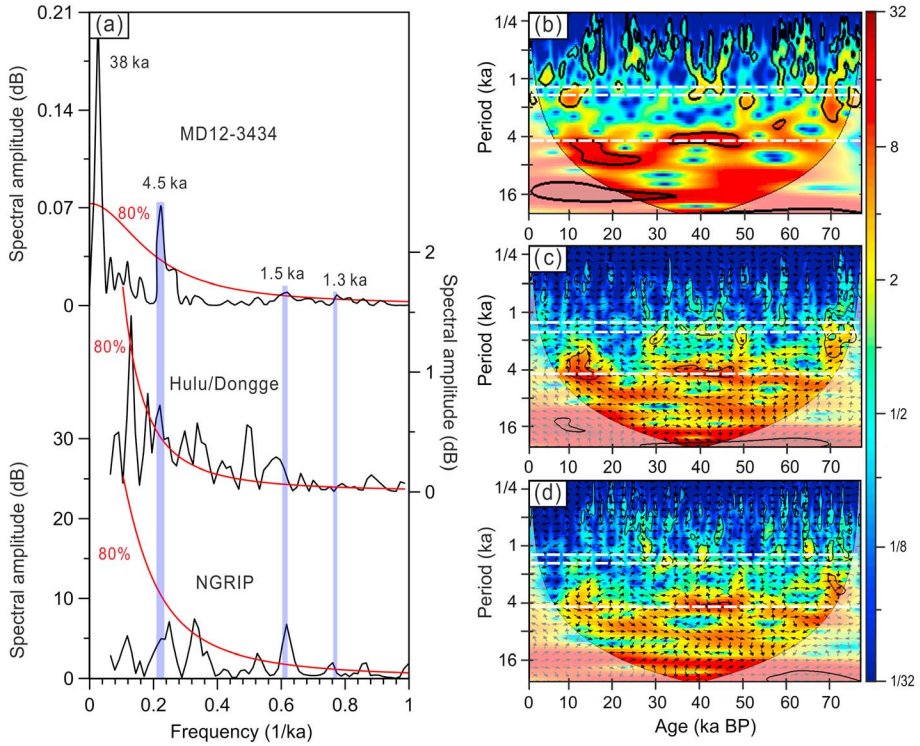

Figure 7. Spectral analysis and continuous wavelet power spectrum for the smectite/(illite + chlorite) ratio of Core MD12-3434 and its cross wavelet analysis with $\delta^{18}O$ records of the Hulu and Dongge cave stalagmites and Greenland NGRIP ice cores. (a) Spectral analysis of Core MD12-3434 smectite/(illite + chlorite) ratio, Hulu and Dongge cave stalagmite $\delta^{18}O$, and Greenland NGRIP ice core $\delta^{18}O$, respectively. The solid red line indicates the 80% confidence level. (b) Continuous wavelet power spectrum for Core MD12-3434 smectite/(illite + chlorite) ratio. (c and d) Cross wavelet transform of Core MD12-3434 smectite/(illite + chlorite) ratio against $\delta^{18}O$ records of Hulu and Dongge cave stalagmites and Greenland NGRIP ice cores, respectively. Three white dashed horizontal lines in (b)–(d) represent the main periods at ~1.3, ~1.5, and ~4.5 ka, respectively. The solid black contours indicate areas with power above the 80% confidence level. Continuous wavelet power spectrum and cross wavelet transform are calculated by the MatLab wavelet coherence package available at http://noc.ac.uk/using-science/crosswavelet-wavelet-coherence (Grinsted et al., 2004).

The clay mineralogical record of Core MD12-3434 in the northern SCS provides a potential linkage between millennial-scale changes in the East Asian monsoon and the North Atlantic climate through a prompt atmospheric teleconnection. The rapid millennial-scale climatic changes occurred in the high-latitude Northern Hemisphere are plausibly linked to the rapid oscillations of the Atlantic Meridional Overturning Circulation (AMOC; e.g., Bond et al., 1993; Herry et al., 2016; McManus et al., 2004). The first possible mechanism for transmitting the rapid millennial-scale climatic change signals from the North Atlantic to East Asia is realized through the northern westerlies (e.g., Guo et al., 1996; Nagashima et al., 2007, 2011; Porter & An, 1995; Sun et al., 2012). A strengthened AMOC during DO and BA interstadials favors leading to a warmer Northern Hemisphere (McManus et al., 2004; Herry et al., 2016), resulting in the weakened westerlies with a remarkable northward shift and enlarged the controlling extent of summer monsoon in East Asia (Nagashima et al., 2007, 2011; Sun et al., 2012). The second possible mechanism is the migration of the ITCZ that could play a significant role in transmitting such millennial-scale climatic change signals from the North Atlantic to the East Asian monsoon region. The ITCZ migrates toward a warmer hemisphere, being dependent on the efficiency of northward energy transport by the AMOC (Schneider et al., 2014). A strengthened AMOC brings more energy to the Northern Hemisphere, leading to both northward shift of the ITCZ and the DO and BA interstadials in the North Atlantic (McManus et al., 2004; Peterson et al., 2000). During this period, the warming Northern Hemisphere favors the relatively strong summer monsoon in East Asia. The prevailing warm and humid climate during strong summer monsoon periods can strengthen the chemical weathering and/or sediment supply under strong physical erosion from Luzon, increasing the smectite export, and further increasing the smectite/(illite + chlorite) ratio in the SCS. On the contrary, an AMOC collapse during

Heinrich and YD stadials tends to result in the southward shift of westerlies and/or the northward migration of the ITCZ, leading to the relatively strong winter monsoon in East Asia. Then, according to the anticorrelation between the East Asian summer monsoon and the East Asian winter monsoon on millennial timescales (Wen et al., 2016), the summer monsoon tends to be weakened during those Heinrich and YD stadials. The prevailing cold air in East Asia tends to decelerate the both chemical and physical weathering rate and/or reduce sediment supply capacity in Luzon, resulting in reduced smectite/(illite + chlorite) ratio in our study core.

Particularly, these millennial-scale changes of the East Asian summer monsoon preserved by clay mineralogical compositions of deep-sea sediments in the SCS tend to be more clear and regular in calm deep-water sedimentary environments. This would explain why several previous records of the SCS semipelagic sediments are less sensitive to the prevailing East Asian monsoon on millennial timescale. To better understand this issue, a compilation of clay mineralogical records located along two transects (T1 and T2) on the northern margin of the SCS have been intercompared (Boulay et al., 2005; Chen et al., 2017; Liu, Li, et al., 2010; Liu et al., 2016; Figures 1b and 8). The smectite/(illite + chlorite) ratios of relatively shallow water Cores MD05-2904, MD05-2905, and MD12-3432 (water depth ~2,000 m) that located along both transects show only the H1 stadial at around 16 ka BP, without other obvious Heinrich stadials or DO interstadials (Chen et al., 2017; Liu, Li, et al., 2010; Liu et al., 2016). By contrast, the smectite/(illite + chlorite) ratios of the deeper-water Core MD12-3434 and ODP Site 1145 (water depth ~3,000 m) display much more clear and regular millennial-scale variations. However, due to the relatively low temporal resolution of ODP Site 1145 smectite/(illite + chlorite) ratio (~780 years; Boulay et al., 2005), it is hard to identify the preserved interstadial DO interstadials on the transect T2. In spite of that, the temporal variations of ODP Site 1145 clay mineralogical ratio correlate well with that of Core MD12-3434, still indicating a better millennial-scale climatic change signals than that preserved in the relatively shallow water Core MD05-2905. This observation has been also convinced by the foraminiferal Mg/Ca-SST records of ODP Sites 1144 and 1145 on the transect T2 (Oppo & Sun, 2005; Wei et al., 2007; Figure 8). Quite obviously, millennial-scale change signals of foraminiferal Mg/Ca-SST at deeper-water ODP Site 1145 are much regular than that of the relatively shallow water ODP Site 1144.

For further constraining the depth-related rapid climatic change signals preserved by clay mineralogy along the two transects, we have adopted a rough quantitative calculation to obtain the amplitudes of their millennial-scale changes. The overall trends of temporal changes in clay mineralogical ratio were estimated by the running average analysis. The relatively higher-resolution data of Cores MD12-3434, MD05-2904, and MD05-2905 were smoothed with a 50-point running average, while the lower-resolution data of Core MD12-3432 and ODP Site 1145 were smoothed only with a 25-point running average (Figure 8). Then, the amplitude of millennial-scale changes in clay mineralogical ratio of each core can be obtained by subtracting the running average values. The results show that on the transect T1, the millennial-scale change amplitude of the relatively deeper-water Core MD12-3434 varies from −0.32 to 0.42 that is larger than both Cores MD12-3432 (from–0.22 to 0.40) and MD05-2904 (from −0.33 to 0.38). This observation can also be convinced on the transect T2; that is, the millennial-scale change amplitude of clay mineralogical ratio of the relatively deeper-water ODP Site 1145 (from −0.26 to 0.52) is clearly larger than that of Core MD05-2905 (from −0.20 to 0.41). In combination with the above discussion of the sedimentary environment changes along the two transects, the relatively small amplitude and low clarity of millennial-scale climatic change signals at the relatively shallow water (~2,000 m) can be possibly ascribed to the disturbance of the contour currents. This strong influence of the contour currents on clay mineralogy can also be peered from the obviously different variation features of smectite/(illite + chlorite) ratio of Cores MD12-3432 and MD05-2904 (Figure 8), though these two cores are located quite close to each other (Figure 1b). In contrast, the increased amplitude of more regular and distinct millennial-scale changes in clay mineralogical ratio in deep water (~3,000 m) have strongly implied that the deep-sea sediments in the relatively calm sedimentary environment can better preserve millennial-scale climatic change information, possibly indicating a very weak influence of the contour currents.

Moreover, temporal variations of Core MD12-3434 smectite/(illite + chlorite) ratio also present long-term orbital changes of the East Asian summer monsoon, which indicate different driving mechanisms by comparison with their millennial-scale changes. First, on the precession timescale, variations of smectite/(illite + chlorite) ratio appear to follow the Northern Hemisphere summer insolation (21 July) at 65°N (Berger, 1978), which is also in common with stalagmite $\delta^{18}O$ records of Hulu and Dongge caves

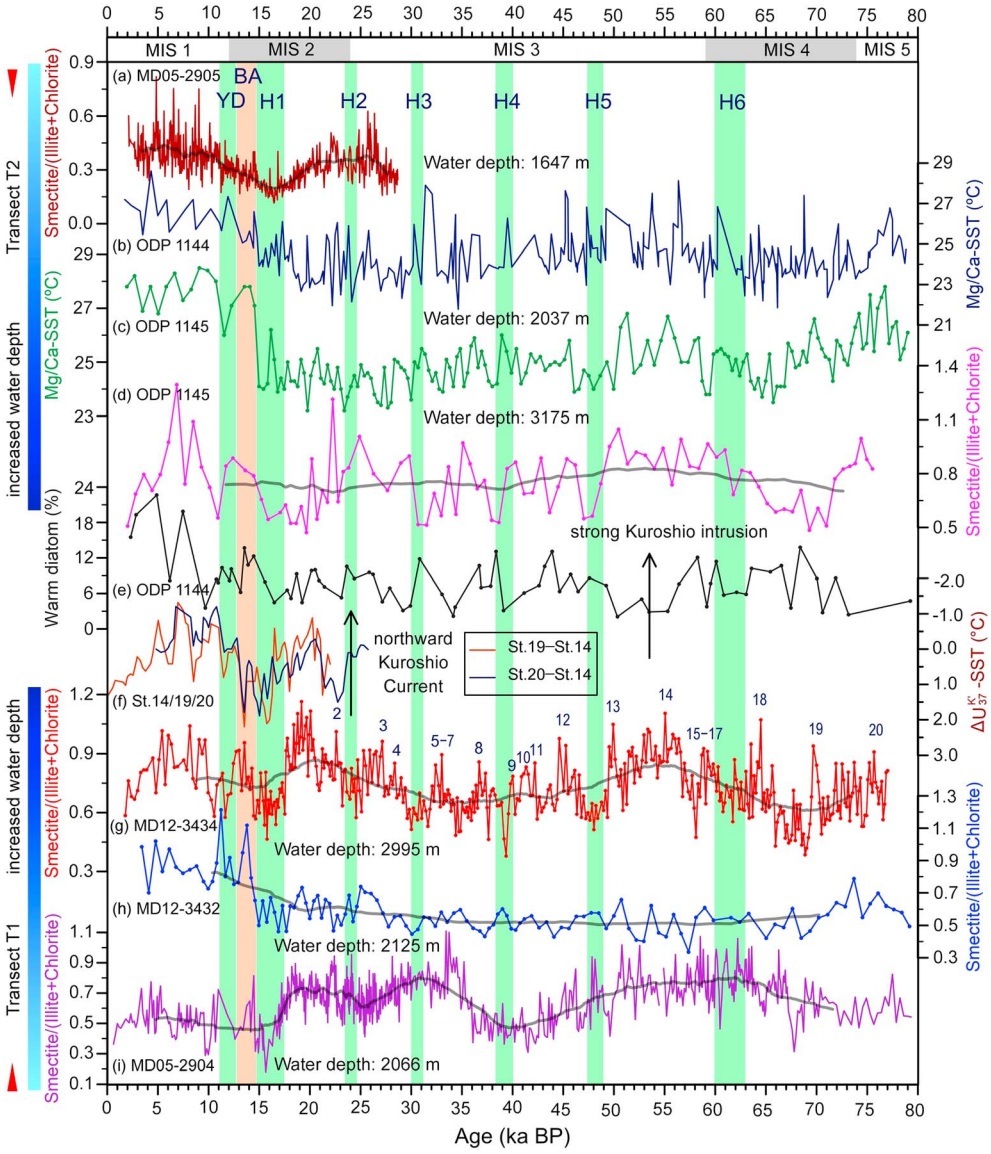

Figure 8. Smectite/(illite + chlorite) ratio of Core MD12-3434 during the last glaciation and their comparison with other paleoenvironmental records in the northern SCS. (a) Smectite/(illite + chlorite) ratio of Core MD05-2905 (Liu ZF, unpublished data); (b) foraminiferal Mg/Ca-SST (sea surface temperature) of ODP Site 1144 (Wei et al., 2007); (c) foraminiferal Mg/Ca-SST of ODP Site 1145 (Oppo & Sun, 2005); (d) Smectite/(illite + chlorite) ratio of ODP Site 1145 (Boulay et al., 2005); (e) warm diatom (%) record of ODP Site 1144 (Jiang et al., 2006); (f) $\Delta U^{K'}_{37}$ SST of (St.19–St.14) and (St.20–St.14) in the coastal area of Japan, respectively (Sawada & Handa, 1998); (g) smectite/(illite + chlorite) ratio of Core MD12-3434 in this study; (h) smectite/(illite + chlorite) ratio of Core MD12-3432 (Chen et al., 2017); (i) smectite/(illite + chlorite) ratio of Core MD05-2904 (Liu et al., 2016). In order to obtain overall trends (gray) of temporal variations, clay mineralogical data of Cores MD12-3434, MD05-2904, and MD05-2905 with relatively higher time resolution are smoothed with a 50-point running average while the lower-resolution data of Core MD12-3432 and ODP Site 1145 are smoothed with a 25-point running average. The records from (a) to (d) and from (g) to (i) show increased water depth variations across transects T2 and T1, respectively. H1–6, YD, BA, and DO events are marked after Y. J. Wang et al. (2001).

(Figure 6). An increased Northern Hemisphere summer insolation normally drives a strong East Asian summer monsoon (Cheng et al., 2016; Wang et al., 2008). Consequently, the increased smectite/(illite + chlorite) ratio on the precession timescale associated with increased summer insolation further implies the enhanced both chemical and physical weathering and/or sediment supply from Luzon under the strengthened summer monsoonal rainfall (Chen et al., 2017). However, the classic precession periodicity (23 ka) for the East Asian summer monsoon evolution that is usually present in the long-term stalagmite $\delta^{18}O$ records of Chinese

caves (Wang et al., 2008; Cheng et al., 2016) is not recognizable in our new clay mineralogical record (Figure 7a). That is possibly because the weak precession forcing coupled with expansion of the Northern Hemisphere ice sheets during the last glaciation may obscure the precession periodicity. Such observations have also been obtained in the stalagmite $\delta^{18}O$ records of Hulu and Dongge caves since the last glaciation (Dykoski et al., 2005; Wang et al., 2001; Figure 7a). Second, the smectite/(illite + chlorite) ratio of Core MD12-3434 also displays a clearly longer periodicity of 38 ka that maybe relates to an obliquity forcing process (Figure 7a). This periodicity can be also confirmed by the clay mineral assemblage variations of ODP Sites 1145 and 1146 in long-term records that present clear periodicities of 38 and 41 ka, respectively (Boulay et al., 2005; Liu et al., 2003). In combination with the absent glacial–interglacial cyclicity of our clay mineralogical record, it is hard to attribute such a longer periodicity to be a true climate change signal if only depending on a record spanning the last two glacial-interglacial cycles.

Additionally, temporal variations of Core MD12-3434 smectite/(illite + chlorite) ratio also display some distinct features different from the $\delta^{18}O$ records of Greenland ice cores and Hulu cave stalagmites, especially during 17.5–23.0 ka BP (between H1 and H2 stadials; Figure 6). The smectite/(illite + chlorite) ratio increases largely in the SCS, while only a slight shift is observed in the $\delta^{18}O$ records of Hulu cave stalagmites and Greenland ice cores. During this time interval, the Kuroshio Current has moved northward deduced from $U^{K'}_{37}$-SST records in the coastal area of Japan, indicating a northward migration of the North Equatorial Current (Sawada & Handa, 1998; Figure 8). This tends to result in a weakened Kuroshio Current off Luzon, but favoring strengthened Kuroshio intrusion into the SCS based on both modern observations and model simulations (Wu, 2013; Wu et al., 2017). As a result, the efficiency of smectite transport from Luzon to Core MD12-3434 could be enhanced, resulting in increase of the smectite/(illite + chlorite) ratio. However, according to a warm diatom (%) record of ODP 1144 Site that is used as the rough potential proxy for Kuroshio intrusion (Jiang et al., 2006; Figure 8), its temporal variation pattern is quite different by comparison with Core MD12-3434 clay mineralogical ratio. Coupling with the fact that a strong Kuroshio intrusion into the SCS normally correlated with an increased winter monsoon (e.g., Hsin et al., 2012; Wu et al., 2017; Wu & Hsin, 2012), this observation has indicated that such influences of Kuroshio intrusion on our clay mineralogical records, reflecting the summer monsoon changes, should be very occasionally. In spite of that, the similar temporal variation pattern of our clay mineralogical ratio and stalagmite $\delta^{18}O$ records of China caves on both millennial and precession timescales has probably indicated that the main controlling factor on clay mineralogical compositions in the northern SCS deep-sea sediments is the prevailing monsoon changes, whereas the influence of oceanic current transport system should be very limited. Nevertheless, our results confirm that clay mineralogy is a powerful tool for tracking the rapid millennial-scale East Asian monsoon variations preserved in the SCS deep-sea sediments. Being compared with other proxies, such as the SST and elemental indexes of terrigenous inputs (Lin et al., 2006; Oppo & Sun, 2005; Wei et al., 2007; Xie et al., 2014; Figure 8), our record provides, for the first time, an excellent mineralogical indicator of the rapid millennial-scale East Asian monsoon evolution in the low-latitude SCS.

5. Conclusions

High-resolution clay mineralogy combined with Nd and Sr isotopic compositions has been investigated at Core MD12-3434 located in the northern SCS to reconstruct rapid millennial-scale changes of the East Asian summer monsoon for the past 78 ka. We draw the following conclusions:

1. The clay mineral assemblage of Core MD12-3434 consists of dominant smectite (25–50%) and illite (25–43%), moderate chlorite (17–27%), and minor kaolinite (3–12%). The temporal variations of smectite, illite, and chlorite contents do not show glacial-interglacial cyclicity but display clear millennial-scale changes. In contrast, kaolinite content has a distinct glacial-interglacial variation pattern. The provenance analysis based on coupled clay mineralogy and Nd and Sr isotopic compositions of terrigenous sediments indicates that clay minerals of Core MD12-3434 are mainly derived from Taiwan and Luzon, with a minor contribution from South China. Taiwan contributes mostly illite and chlorite, while Luzon and South China contributes smectite and kaolinite, respectively.
2. As the contribution of smectite deriving from rapid chemical weathering of volcanic rocks and/or sediment supply under strong physical erosion from Luzon during the intervals of strengthened summer monsoonal rainfall, the smectite/(illite + chlorite) ratio of Core MD12-3434 is adopted as a robust

mineralogical proxy for tracking the millennial-scale evolution history of the East Asian summer monsoon. During the last glaciation, rapid increases in smectite/(illite + chlorite) ratios imply strengthened summer monsoonal rainfall occurred during DO and BA interstadials, while rapid decreases in smectite/(illite + chlorite) ratios indicate relatively weakened summer monsoon conditions happened during Heinrich and YD stadials. Such results highlight the prompt responses of the East Asian monsoon system to rapid millennial-scale climatic changes occurred in high-latitude Greenland through contemporaneous chemical weathering of volcanic rocks and/or sediment supply under strong physical erosion in the low-latitude areas.

3. Millennial-scale changes of the East Asian summer monsoon documented by clay mineralogical compositions of deep-sea sediments in the SCS can be better preserved in calm deep-water sedimentary environments.

Acknowledgments
We would like to thank the captain, officers, and crew of R/V Marion Dufresne for their cooperation in collecting sediment cores during the CIRCEA cruise in 2012. Gert J. de Lange (Utrecht University) is appreciated for his constructive comments that help to improve this paper. The work is financially supported by the National Natural Science Foundation of China (91528304 and 41530964) and the State Oceanic Administration of China (GASI-GEOGE-04). The study is a part of the French-Chinese collaborative project of International Associated Laboratories (LIA) MONOCL. The clay mineralogical data used in this paper can be found in the supporting information.

References

Ali, S., Hathorne, E., Frank, M., Gebregiorgis, D., Stattegger, K., Stumpf, R., et al. (2015). South Asian monsoon history over the past 60 kyr recorded by radiogenic isotopes and clay mineral assemblages in the Andaman Sea. *Geochemistry, Geophysics, Geosystems*, *16*, 505–521. https://doi.org/10.1002/2014GC005586

Beaulieu, E., Goddéris, Y., Donnadieu, Y., Labat, D., & Roeland, C. (2012). High sensitivity of the continental-weathering carbon dioxide sink to future climate change. *Nature Climate Change*, *2*, 346–349.

Berger, A. (1978). Long-term variations of caloric insolation resulting from the Earth's orbital elements. *Quaternary Research*, *9*(02), 139–167. https://doi.org/10.1016/0033-5894(78)90064-9

Biscaye, P. (1965). Mineralogy and sedimentation of recent deep-sea clay in the Atlantic Ocean and adjacent seas and oceans. *Geological Society of America Bulletin*, *76*(7), 803–832. https://doi.org/10.1130/0016-7606(1965)76[803:MASORD]2.0.CO;2

Black, D., Haneed, S., & Peterson, L. (2009). Long-term tidal cycle influences on a late-Holocene clay mineralogy record from the Cariaco Basin. *Earth and Planetary Science Letters*, *279*, 139–146.

Blunier, T., Chappellaz, J., Schwander, J., Dällenbach, A., Stauffer, B., Stocker, T., et al. (1998). Asynchrony of Antarctic and Greenland climate change during the last glacial period. *Nature*, *394*(6695), 739–743. https://doi.org/10.1038/29447

Bond, G., Broecker, W., Johnsen, S., McManus, J., Labeyrie, L., Jouzel, J., & Bonani, G. (1993). Correlations between climate records from North Atlantic sediments and Greeland ice. *Nature*, *365*, 143–147.

Boulay, S., Colin, C., Trentesaux, A., Frank, N., & Liu, Z. F. (2005). Sediment sources and East Asian monsoon intensity over the last 450 kyr: mineralogical and geochemical investigations on South China Sea sediment. *Palaeogeography Palaeoclimatology Palaeoecology*, *228*, 260–277.

Chang, Y.-P., Chen, M.-T., Yokoyama, Y., Matsuzaki, H., Thompson, W., Kao, S.-J., & Kawahata, H. (2009). Monsoon hydrography and productivity changes in the East China Sea during the past 100,000 years: Okinawa Trough evidence (MD012404). *Paleoceanography*, *24*, PA3208. https://doi.org/10.1029/2007PA001577

Chen, Q., Liu, Z. F., & Kissel, C. (2017). Clay mineralogical and geochemical proxies of the East Asian summer monsoon evolution in the South China Sea during Late Quaternary. *Scientific Reports*, *7*, 42083. https://doi.org/10.1038/srep42083

Cheng, H., Edwards, R., Sinha, A., Spötl, C., Yi, L., Chen, S. T., et al. (2016). The Asian monsoon over the past 640,000 years and ice age terminations. *Nature*, *534*(7609), 640–646. https://doi.org/10.1038/nature18591

Clift, P., Wan, S. M., & Blusztajn, J. (2014). Reconstructing chemical weathering, physical erosion and monsoon intensity since 25 Ma in the northern South China Sea: A review of competing proxies. *Earth Science Reviews*, *130*, 86–102. https://doi.org/10.1016/j.earscirev.2014.01.002

Colin, C., Siani, G., Liu, Z. F., Blamart, B., Skonieczny, C., Zhao, Y. L., et al. (2014). Late Miocene to early Pliocene climate variability off NW Africa (ODP Site 659). *Palaeogeography Palaeoclimatology Palaeoecology*, *40*, 81–95.

Copard, K., Colin, C., Douville, E., Freiwald, A., Gudmundsson, G., De Mol, B., & Frank, N. (2010). Nd isotopes in deep-sea corals in the North-eastern Atlantic. *Quaternary Science Reviews*, *29*(19-20), 2499–2508. https://doi.org/10.1016/j.quascirev.2010.05.025

Dadson, S., Hovius, N., Chen, H., Dade, W., Hsieh, M., Willett, S., et al. (2003). Links between erosion, runoff variability and seismicity in the Taiwan orogen. *Nature*, *426*(6967), 648–651. https://doi.org/10.1038/nature02150

Dansgaard, W., Johnsen, S., Clausen, H., Hahl-Jensen, D., Gundestrup, N., Hammer, C., et al. (1993). Evidence for general instability of past climate from a 250 kyr ice-core record. *Nature*, *364*(6434), 218–220. https://doi.org/10.1038/364218a0

Deplazes, G., Lückge, A., Peterson, L., Timmermann, A., Hamann, Y., Hughen, K., et al. (2013). Links between tropical rainfall and North Atlantic climate during the last glacial period. *Nature Geoscience*, *6*(3), 213–217. https://doi.org/10.1038/ngeo1712

Ding, X. D., Zheng, L. W., Li, D. W., Yang, T.-N., Lee, T.-Q., & Kao, S.-J. (2016). Lacustrine record of centennial- and millennial-scale rainfall variability of the East Asian summer monsoon during the last deglaciation: Multi-proxy evidence from Taiwan. *Palaeogeography, Palaeoclimatology, Palaeoecology*, *450*, 38–49. https://doi.org/10.1016/j.palaeo.2016.02.048

Dosseto, A., Vigier, N., Joannes-Boyau, R., Moffat, I., Singh, T., & Srivastava, P. (2015). Rapid response of silicate weathering rates to climate change in the Himalaya. *Geochemical Perspectives Letters*, *1*, 10–19.

Dykoski, C., Edwards, R., Cheng, H., Yuan, D. X., Cai, Y. J., Zhang, M. L., et al. (2005). A high-resolution, absolute-dated Holocene and deglacial Asian monsoon record from Dongge Cave, China. *Earth and Planetary Science Letters*, *233*, 71–86.

Fang, G. H., Fang, W. D., Fang, Y., & Wang, K. (1998). A survey of studies on the South China Sea upper ocean circulation. *Acta Oceanographica Taiwanica*, *37*(1), 1–16.

Gislason, S., Oelkers, E., Eiriksdottir, E., Kardjilov, M., Gisladottir, G., Sigfusson, B., et al. (2009). Direct evidence of the feedback between climate and weathering. *Earth and Planetary Science Letters*, *277*(1-2), 213–222. https://doi.org/10.1016/j.epsl.2008.10.018

Grinsted, A., Moore, J., & Jevrejeva, S. (2004). Application of the cross wavelet transform and wavelet coherence to geophysical time series. *Nonlinear Processes in Geophysics*, *11*(5/6), 561–566. https://doi.org/10.5194/npg-11-561-2004

Guo, Z. T., Liu, T.-S., Guiot, J., Wu, N., Lü, H., Han, J., et al. (1996). High frequency pulses of East Asia monsoon climate in the last two glaciations: Link with the North Atlantic. *Climate Dynamics*, *12*(10), 701–709. https://doi.org/10.1007/s003820050137

Hartshorn, K., Hovius, N., Dade, W., & Slingerland, R. (2002). Climate-driven bedrock incision in an active mountain belt. *Science*, *297*(5589), 2036–2038. https://doi.org/10.1126/science.1075078

Heinrich, H. (1988). Origin and consequence of cyclic ice rafting in the northeast Atlantic Ocean during the past 130000 years. *Quaternary Research*, *29*(02), 142–152. https://doi.org/10.1016/0033-5894(88)90057-9

Herry, L., McManus, J., Curry, W., Roberts, N., Piotrowski, A., & Keigwin, L. (2016). North Atlantic ocean circulation and abrupt climate change during the last glaciation. *Science*, *353*(6298), 470–474.

Holtzapffel, T. (1985). Les Minéraux Argileux: Préparation, Analyse Diffractométrique et Determination. *Society Géological Nord Publication*, *12*, 1–136.

Hsin, Y.-C., Wu, C.-R., & Chao, S.-Y. (2012). An updated examination of the Luzon Strait transport. *Journal of Geophysical Research*, *117*, C03022. https://doi.org/10.1029/2011JC007714

Hu, D. K., Clift, P., Böning, P., Hannigan, R., Hillier, S., Blusztajn, J., et al. (2013). Holocene evolution in weathering and erosion patterns in the Pearl River delta. *Geochemistry, Geophysics, Geosystems*, *14*, 2349–2368. https://doi.org/10.1002/ggge.20166

Hu, J. Y., Kawamura, H., Hong, H. S., & Qi, Y. Q. (2000). A review on the currents in the South China Sea: Seasonal circulation, South China Sea Warm Current and Kuroshio intrusion. *Journal of Oceanography*, *56*(6), 607–624. https://doi.org/10.1023/A:1011117531252

Huang, J., Li, A. C., & Wan, S. M. (2011). Sensitive grain-size records of Holocene East Asian summer monsoon in sediments of northern South China Sea slope. *Quaternary Research*, *75*, 734–744.

Jacobsen, S., & Wasserburg, G. (1980). Sm-Nd isotopic evolution of chondrites. *Earth and Planetary Science Letters*, *50*, 139–155.

Jiang, H., Björk, S., Ran, L. H., Huang, Y., & Li, J. Y. (2006). Impact of the Kuroshio current on the South China Sea based on a 115 000 year diatom record. *Journal of Quaternary Science*, *21*(4), 377–385. https://doi.org/10.1002/jqs.1000

Kissel, C., Jian, Z. M., Leau, H., and the Shipboard Scientific Party (2012). MD190-CIRCEA cruise report, in: Les rapports de campagne à la mer, IPEV, ref: OCE/2012/01.

Li, N., Yang, X. Q., Peng, J., Zhou, Q. X., & Su, Z. H. (2017). Deep-water bottom current evolution in the northern South China Sea during the last 150 kyr: Evidence from sortable-silt grain size and sedimentary magnetic fabric. *Journal of Asian Earth Sciences*. https://doi.org/10.1016/j.jseaes.2017.06.005

Lin, D.-C., Chen, M.-T., Murayama, M., & Yokoyama, Y. (2014). Millennial-scale alkenone sea surface temperature changes in the northern South China Sea during the past 45,000 years (MD972146). *Quaternary International*, *333*, 207–215. https://doi.org/10.1016/j.quaint.2014.03.062

Lin, D.-C., Liu, C.-H., Fang, T.-H., Tsai, C.-H., Murayama, M., & Chen, M.-T. (2006). Millennial-scale changes in terrestrial sediment input and Holocene surface hydrography in the northern South China Sea (IMAGES MD972146). *Palaeogeography Palaeoclimatology Palaeoecology*, *236*(1-2), 56–73. https://doi.org/10.1016/j.palaeo.2005.11.039

Liu, J. G., Yan, W., Chen, Z., Chen, H., & Lu, J. (2014). Comment on "Holocene evolution in weathering and erosion patterns in the Pearl River delta" by Hu et al. *Geochemistry, Geophysics, Geosystems*, *15*, 2727–2731. https://doi.org/10.1002/2013GC005202

Liu, Z. F., Colin, C., Huang, W., Le, K. P., Tong, S. Q., Chen, Z., & Trentesaux, A. (2007). Climatic and tectonic controls on weathering in South China and the Indochina Peninsula: Clay mineralogical and geochemical investigations from the Pearl, Red, and Mekong drainage basins. *Geochemistry, Geophysics, Geosystems*, *8*, Q05005. https://doi.org/10.1029/2006GC001490

Liu, Z. F., Colin, C., Li, X. J., Zhao, Y. L., Tuo, S. T., Chen, Z., et al. (2010). Clay mineral distribution in surface sediments of the northeastern South China Sea and surrounding fluvial drainage basins: Source and transport. *Marine Geology*, *277*(1-4), 48–60. https://doi.org/10.1016/j.margeo.2010.08.010

Liu, Z. F., Colin, C., Trentesaux, A., Blamart, D., Bassinot, F., Siani, G., & Sicre, M.-A. (2004). Erosional history of the eastern Tibetan Plateau since 190 kyr ago: Clay mineralogical and geochemical investigations from the southwestern South China Sea. *Marine Geology*, *209*(1-4), 1–18. https://doi.org/10.1016/j.margeo.2004.06.004

Liu, Z. F., Li, X. J., Colin, C., & Ge, H. M. (2010). A high-resolution clay mineralogical record in the northern South China Sea since the Last Glacial Maximum, and its time series provenance analysis. *Chinese Science Bulletin*, *55*(35), 4058–4068. https://doi.org/10.1007/s11434-010-4149-5

Liu, Z. F., & Stattegger, K. (2014). South China Sea fluvial sediments: An introduction. *Journal of Asian Earth Sciences*, *79*, 507–508. https://doi.org/10.1016/j.jseaes.2013.11.003

Liu, Z. F., Trentesaux, A., Clemens, S., Colin, C., Wang, P. X., Huang, B. Q., & Boulay, S. (2003). Clay mineral assemblages in the northern South China Sea: Implications for East Asian monsoon evolution over the past 2 million years. *Marine Geology*, *201*(1-3), 133–146. https://doi.org/10.1016/S0025-3227(03)00213-5

Liu, Z. F., Tuo, S. T., Colin, C., Liu, J. T., Huang, C.-Y., Selvaraj, K., et al. (2008). Detrital fine-grained sediment contribution from Taiwan to the northern South China Sea and its relation to regional ocean circulation. *Marine Geology*, *255*(3-4), 149–155. https://doi.org/10.1016/j.margeo.2008.08.003

Liu, Z. F., Zhao, Y. L., Colin, C., Siringan, F., & Wu, Q. (2009). Chemical weathering in Luzon, Philippines from clay mineralogy and major-element geochemistry of river sediments. *Applied Geochemistry*, *24*(11), 2195–2205. https://doi.org/10.1016/j.apgeochem.2009.09.025

Liu, Z. F., Zhao, Y. L., Colin, C., Stattegger, K., Wiesner, M., Huh, C.-A., et al. (2016). Source-to-Sink transport process of fluvial sediments in the South China Sea. *Earth Science Reviews*, *153*, 238–273. https://doi.org/10.1016/j.earscirev.2015.08.005

Markle, B., Steig, E., Buizert, C., Schoenemann, S., Bitz, C., Fudge, T., et al. (2017). Global atmospheric teleconnections during Dansgaard–Oeschger events. *Nature Geoscience*, *10*(1), 36–40. https://doi.org/10.1038/ngeo2848

McManus, J., Francois, R., Gherardi, J.-M., Keigwin, L., & Brown-Leger, S. (2004). Collapse and rapid resumption of Atlantic meridional circulation linked to deglacial climate changes. *Nature*, *428*(6985), 834–837. https://doi.org/10.1038/nature02494

Nagashima, K., Tada, R., Matsui, H., Irino, T., Tani, A., & Toyoda, S. (2007). Orbital- and millennial-scale variations in Asian dust transport path to the Japan Sea. *Palaeogeography Palaeoclimatology Palaeoecology*, *247*(1-2), 144–161. https://doi.org/10.1016/j.palaeo.2006.11.027

Nagashima, K., Tada, R., Tani, A., Sun, Y., Isozaki, Y., Toyoda, S., & Hasegawa, H. (2011). Millennial-scale oscillations of the westerly jet path during the last glacial period. *Journal of Asian Earth Sciences*, *40*(6), 1214–1220. https://doi.org/10.1016/j.jseaes.2010.08.010

North Greenland Ice Core Project Members (2004). High-resolution record of Northern Hemisphere climate extending into the last interglacial period. *Science*, *431*, 147–151.

Oppo, D., & Sun, Y. B. (2005). Amplitude and timing of sea-surface temperature change in the northern South China Sea: Dynamic link to the East Asian monsoon. *Geology*, *33*(10), 785–788. https://doi.org/10.1130/G21867.1

Partin, J. W., Quinn, T. M., Shen, C.-C., Okumura, Y., Cardenas, M. B., iringan, F. P., et al. (2015). Gradual onset and recovery of the Younger Dryas abrupt climate event in the tropics. *Nature Communications*, *6*(1), 8061. https://doi.org/10.1038/ncomms9061

Peterson, L., Haug, G., Hughen, K., & Röhl, U. (2000). Rapid changes in the hydrologic cycle of the tropical Atlantic during the last glacial. *Science*, *290*, 1947–1951.

Petschick, R. (2000). MacDiff 4.2.2. Retrieved from http://servermac.geologie.un-frankfurt.de/Rainer.html

Porter, S., & An, Z. S. (1995). Correlation between climate events in the North-Atlantic and China during the last glaciation. *Nature*, *375*(6529), 305–308. https://doi.org/10.1038/375305a0

Reimer, P., Bard, E., Bayliss, A., Beck, J., Blackwell, P., Ramsey, C., et al. (2013). IntCal13 and Marine13 radiocarbon age calibration curves 0–50,000 years cal BP. *Radiocarbon*, *55*(4), 1869–1887.

Riboulleau, A., Bout-Roumazeilles, V., & Tribovillard, N. (2014). Controls on detrital sedimentation in the Cariaco Basin during the last climatic cycle: Insight from clay minerals. *Quaternary Science Reviews*, *94*, 62–73. https://doi.org/10.1016/j.quascirev.2014.04.023

Sabatier, P., Dezileau, L., Briqueu, L., Colin, C., & Siani, G. (2010). Clay minerals and geochemistry record from northwestern Mediterranean coastal lagoon sequence: Implications for paleostorm reconstruction. *Sedimentary Geology*, *228*(3-4), 205–217. https://doi.org/10.1016/j.sedgeo.2010.04.012

Sawada, K., & Handa, N. (1998). Variability of the path of the Kuroshio Ocean current over the past 25,000 years. *Nature*, *392*(6676), 592–595. https://doi.org/10.1038/33391

Schmidt, M., Chang, P., Hertzberg, J., Them, T. II, Ji, L., & Otto-Bliesner, B. (2012). Impact of abrupt deglacial climate change on tropical Atlantic subsurface temperatures. *Proceedings of the National Academy of Sciences of the United States of America*, *109*(36), 14,348–14,352. https://doi.org/10.1073/pnas.1207806109

Schneider, T., Bischoff, T., & Haug, G. (2014). Migrations and dynamics of the Intertropical Convergence Zone. *Nature*, *513*(7516), 45–53. https://doi.org/10.1038/nature13636

Schopka, H., Derry, L., & Arcilla, C. (2011). Chemical weathering, river geochemistry and atmospheric carbon fluxes from volcanic and ultramafic regions on Luzon Island, the Philippines. *Geochimica et Cosmochimica Acta*, *75*(4), 978–1002. https://doi.org/10.1016/j.gca.2010.11.014

Schroeder, A., Wiesner, M., & Liu, Z. F. (2015). Fluxes of clay minerals in the South China Sea. *Earth and Planetary Science Letters*, *430*, 30–42. https://doi.org/10.1016/j.epsl.2015.08.001

Selvaraj, K., & Chen, C.-T. (2006). Moderate chemical weathering of subtropical Taiwan: Constraints from solid-phase geochemistry of sediment and sedimentary rocks. *Journal of Geology*, *114*(1), 101–116. https://doi.org/10.1086/498102

Sun, Y. B., Clemens, S., Morrill, C., Lin, X. P., Wang, X. L., & An, Z. S. (2012). Influence of Atlantic meridional overturning circulation on the east Asian winter monsoon. *Nature Geoscience*, *5*, 46–49.

Tada, R. (2004). Onset and evolution of millennial-scale variability in Asian monsoon and its impact on paleoceanography of the Japan Sea. In P. D. Clift, et al. (Eds.), *Continent–Ocean Interactions Within East Asian Marginal Seas*, *Geophysical Monograph Series* (Vol. 149, pp. 283–298). Washington, DC: American Geophysical Union. https://doi.org/10.1029/149GM15

Tada, R., Irino, T., & Koizumi, I. (1999). Land–ocean linkages over orbital and millennial timescales recorded in late Quaternary sediments of the Japan Sea. *Paleoceanography*, *14*(2), 236–247. https://doi.org/10.1029/1998PA900016

Tjallingii, R., Claussen, M., Stuut, J.-B., Fohlmeister, J., Jahn, A., Bickert, T., et al. (2008). Coherent high- and low-latitude control of the northwest African hydrological balance. *Nature Geoscience*, *1*, 670–675.

Wan, S. M., Li, A. C., Clift, P., & Stuut, J.-B. (2007). Development of the East Asian monsoon: Mineralogical and sedimentologic records in the northern South China Sea since 20 ma. *Palaeogeography Palaeoclimatology Palaeoecology*, *254*(3-4), 561–582. https://doi.org/10.1016/j.palaeo.2007.07.009

Wang, B., Wu, Z. W., Li, J. P., Liu, J., Chang, C.-P., Ding, Y. H., & Wu, G. X. (2008). How to measure the strength of the East Asian summer monsoon. *Journal of Climate*, *21*(17), 4449–4463. https://doi.org/10.1175/2008JCLI2183.1

Wang, L. J., Sarnthein, M., Erlenkeuser, H., Grimalt, J., Grootes, P., Heilig, S., et al. (1999). East Asian monsoon climate during the late Pleistocene: High-resolution sediment records from the South China Sea. *Marine Geology*, *156*(1-4), 245–284. https://doi.org/10.1016/S0025-3227(98)00182-0

Wang, L. J., & Wang, P. X. (1990). Late Quaternary paleoceanography of the South China Sea: Glacial-interglacial contrasts in an enclosed basin. *Paleoceanography*, *5*(1), 77–90. https://doi.org/10.1029/PA005i001p00077

Wang, P. X., Li, Q. Y., & Tian, J. (2014). Pleistocene paleoceanography of the South China Sea: Progress over the past 20 years. *Marine Geology*, *352*, 381–396. https://doi.org/10.1016/j.margeo.2014.03.003

Wang, P. X., Wang, B., Cheng, H., Fasullo, J., Guo, Z. T., Kiefer, T., & Liu, Z. Y. (2014). The global monsoon across time scales: Coherent variability of regional monsoons. *Climate of the Past*, *10*(1), 1–19. https://doi.org/10.5194/cp-10-1-2014

Wang, P. X., Wang, B., Cheng, H., Fasullo, J., Guo, Z. T., Kiefer, T., & Liu, Z. Y. (2017). The global monsoon across time scales: Mechanisms and outstanding issues. *Earth Science Reviews*, *174*, 84–121. https://doi.org/10.1016/j.earscirev.2017.07.006

Wang, X. X. (2015). Paleoceanographic changes and its impact on air-sea CO_2 exchange in the northern South China Sea since the last glaciation. Master Thesis. Tongji University.

Wang, Y. J., Cheng, H., Edwards, R., An, Z. S., Wu, J. Y., Shen, C.-C., & Dorale, J. (2001). A high-resolution absolute-dated late Pleistocene monsoon record from Hulu Cave, China. *Science*, *294*(5550), 2345–2348. https://doi.org/10.1126/science.1064618

Wang, Y. J., Cheng, H., Edwards, R., Kong, X. G., Shao, X. H., Chen, S. T., et al. (2008). Millennial- and orbital-scale changes in the East Asian monsoon over the past 224,000 years. *Nature*, *451*(7182), 1090–1093. https://doi.org/10.1038/nature06692

Wei, G. J., Deng, W. F., Liu, Y., & Li, X. H. (2007). High-resolution sea surface temperature records derived from foraminiferal Mg/Ca ratios during the last 260 ka in the northern South China Sea. *Palaeogeography Palaeoclimatology Palaeoecology*, *250*(1-4), 126–138. https://doi.org/10.1016/j.palaeo.2007.03.005

Wen, X. Y., Liu, Z. Y., Wang, S. W., Cheng, J., & Zhu, J. (2016). Correlation and anti-correlation of the East Asian summer and winter monsoons during the last 21,000 years. *Nature Communications*, *7*, 11999. https://doi.org/10.1038/ncomms11999

Wu, C.-R. (2013). Interannual modulation of the Pacific Decadal Oscillation (PDO) on the low-latitude western North Pacific. *Progress in Oceanography*, *110*, 49–58. https://doi.org/10.1016/j.pocean.2012.12.001

Wu, C.-R., & Hsin, Y.-C. (2012). The forcing mechanism leading to the Kuroshio intrusion into the South China Sea. *Journal of Geophysical Research*, *117*, C07015. https://doi.org/10.1029/2012JC007968

Wu, C.-R., Wang, Y.-L., Lin, Y.-F., & Chao, S.-Y. (2017). Intrusion of the Kuroshio into the South and East China Seas. *Scientific Reports*, *7*, 7895. https://doi.org/10.1038/s41598-017-08206-4

Xie, X., Zheng, H. B., & Qiao, P. J. (2014). Millennial climate changes since MIS 3 revealed by element records in deep sea sediments from northern South China Sea. *Chinese Science Bulletin*, *59*, 776–784.

Yu, Z. J., Wan, S. M., Colin, C., Yan, H., Bonneau, L., Liu, Z. F., et al. (2016). Co-evolution of monsoonal precipitation in East Asia and the tropical Pacific ENSO system since 2.36 Ma: New insights from high-resolution clay mineral records in the West Philippine Sea. *Earth and Planetary Science Letters*, *446*, 45–55.

Zhao, M. X., Huang, C.-Y., Wang, C.-C., & Wei, G. J. (2006). A millennial-scale $U^{K'}_{37}$ sea-surface temperature record from the South China Sea (8°N) over the last 150 kyr: Monsoon and sea-level influence. *Palaeogeography Palaeoclimatology Palaeoecology*, *236*, 39–55.

Zhao, S. H., Liu, Z. F., Chen, Q., Wang, X. X., Shi, J. N., Liu, J. J., & Jian, Z. M. (2017). Spatiotemporal variations of deep-sea sediment components and their fluxes since the last glaciation in the northern South China Sea. *Science China Earth Sciences*, *60*(7), 1368–1381. https://doi.org/10.1007/s11430-016-9058-6

Zhao, W., Zhou, C., Tian, J. W., Yang, Q. X., Wang, B., Xie, L. L., & Qu, T. D. (2014). Deep water circulation in the Luzon Strait. *Journal of Geophysical Research*, *119*, 790–804. https://doi.org/10.1002/2013JC009587

Zhao, Y. L., Liu, Z. F., Zhang, Y. W., Li, J. R., Wang, M., Wang, W. G., & Xu, J. P. (2015). In situ observation of contour currents in the northern South China Sea: Applications for deepwater sediment transport. *Earth and Planetary Science Letters*, *430*, 477–485. https://doi.org/10.1016/j.epsl.2015.09.008

Zheng, X. F., Kao, S.-J., Chen, Z., Menviel, L., Chen, H., Du, Y., et al. (2016). Deepwater circulation variation in the South China Sea since the Last Glacial Maximum. *Geophysical Research Letters*, *43*, 8590–8599. https://doi.org/10.1002/2016GL070342

Zhong, Y., Chen, Z., Li, L., Liu, J. G., Li, G., Zheng, X. F., et al. (2017). Bottom water hydrodynamic provinces and transport patterns of the northern South China Sea: Evidence from grain size of the terrigenous sediments. *Continental Shelf Research*, *40*, 11−26.